Mon. Not. R. Astron. Soc. **327,** 918–938 (2001)

Using the Ca II triplet to trace abundance variations in individual red giant branch stars in three nearby galaxies

Eline Tolstoy,[1★]† Michael J. Irwin,[2★] Andrew A. Cole,[3★] L. Pasquini,[4★] R. Gilmozzi[4★] and J. S. Gallagher[5★]

[1]*UK Gemini Support Group, Nuclear and Astrophysics Laboratory, University of Oxford, Keble Road, Oxford OX1 3RH*
[2]*Institute of Astronomy, University of Cambridge, Madingley Road, Cambridge CB3 0HA*
[3]*Department of Astronomy, 532A LGRT, University of Massachusetts, Amherst, MA 01003, USA*
[4]*European Southern Observatory, Karl-Schwarzschild str. 2, 85748 Garching bei München, Germany*
[5]*Department of Astronomy, University of Wisconsin–Madison, 475 North Charter Street, Madison, WI 53706, USA*

Accepted 2001 June 28. Received 2001 June 26; in original form 2001 April 2

ABSTRACT

Spectroscopic abundance determinations for stars spanning a Hubble time in age are necessary in order to determine unambiguously the evolutionary histories of galaxies. Using FORS1 in multi-object spectroscopy mode on ANTU (UT1) at the ESO VLT on Paranal, we have obtained near-infrared spectra from which we have measured the equivalent widths of the two strongest Ca II triplet lines to determine metal abundances for a sample of red giant branch stars, selected from ESO NTT optical (I, $V-I$) photometry of three nearby Local Group galaxies: the Sculptor dwarf spheroidal, the Fornax dwarf spheroidal and the dwarf irregular NGC 6822. The summed equivalent width of the two strongest lines in the Ca II triplet absorption-line feature, centred at 8500 Å, can be readily converted into an [Fe/H] abundance using the previously established calibrations by Armandroff & Da Costa and Rutledge, Hesser & Stetson. We have measured metallicities for 37 stars in Sculptor, 32 stars in Fornax and 23 stars in NGC 6822, yielding more precise estimates of the metallicity distribution functions for these galaxies than it is possible to obtain photometrically. In the case of NGC 6822, this is the first direct measurement of the abundances of the intermediate-age and old stellar populations. We find metallicity spreads in each galaxy which are broadly consistent with the photometric width of the red giant branch, although the abundances of individual stars do not always appear to correspond to their colour. This is almost certainly predominantly due to a highly variable star formation rate with time in these galaxies, which results in a non-uniform, non-globular-cluster-like evolution of the Ca/Fe ratio.

Key words: galaxies: individual: Sculptor – galaxies: individual: Fornax – galaxies: individual: NGC 6822 – galaxies: kinematics and dynamics – Local Group – infrared: galaxies.

1 INTRODUCTION

It is impossible to determine the star formation history of a galaxy uniquely on the basis of photometry of individual red giant branch (RGB) stars alone. This is because the uncertainty in the metallicity (heavy element abundance) of a star translates into an uncertainty in age. This is the age–metallicity degeneracy which plagues the accurate analysis of colour–magnitude diagram (CMDs) (e.g. Searle, Wilkinson & Bagnuolo 1980; Tolstoy 1998, and references therein; Cole et al. 1999). It is necessary to measure directly the abundance of stars of different ages to understand how metallicity has changed with time. This has not been easily possible for galaxies beyond the Magellanic Clouds until the advent of 8-m-class telescopes, even at the intermediate resolutions required for the most basic of metallicity indicators, the Ca II triplet. Looking at isolated systems beyond our rather complex immediate neighbourhood means that we can avoid the difficult interpretations required to understand the properties of our Galaxy (e.g. Edvardsson et al. 1993) and the Magellanic Clouds (e.g. Olszewski et al. 1991; Da Costa & Hatzidimitriou 1998; Cole,

★E-mail: etolstoy@astro.rug.nl (ET); mike@ast.cam.ac.uk (MJI); cole@condor.astro.umass.edu (AAC); lpasquin@eso.org (LP); rgilmozz@eso.org (RG); jsg@astro.wisc.edu (JSG)
†Present address: Kapteyn Institute, Postbus 800, 9700AV Groningen, the Netherlands.

Table 1. The galaxy sample.

Object	l	b	V(HB)	$(m-M)_0$	$E(B-V)$	M_V	v_r	σ (km s^{-1})	Type	Ref.
Sculptor	287.5	−83.2	20.35	19.54 ± 0.08	0.02 ± 0.02	−11.1	110	6	dSph	1,2,6,8
Fornax	237.1	−65.7	21.50	20.70 ± 0.12	0.03 ± 0.01	−13.2	53	10	dSph	3,4,6,9
NGC 6822	25.3	−18.4	24.6:	23.45 ± 0.15	0.26 ± 0.04	−15.2	−49	−	dI	5,6,7

References: (1) Kunkel & Demers (1977); (2) Majewski et al. (1999); (3) Beauchamp et al. (1995); (4) Buonanno et al. (1999); (5)Gallart et al. (1996a); (6) Mateo (1998); (7) Wyder, Hodge & Zucker (2000); (8) Queloz, Dubath & Pasquini (1995); (9) Mateo et al. (1991).

Table 2. Calibration globular clusters.

Object	l	b	[Fe/H]	$E(B-V)$	V(HB)	$(m-M)_V$	v_r (km s^{-1})
47 Tuc	305.9	−44.9	−0.71	0.04	14.06	13.37	−18.7
Pal 12	30.5	−47.7	−1.00	0.02	17.13	16.47	+27.8
Rup 106	300.9	11.7	−1.45	0.20	17.80	17.25	−44.0
M15	65.0	−27.3	−2.15	0.10	15.83	15.37	−107.3

Smecker-Hane & Gallagher 2000), and find systems that are simpler and thus (hopefully) easier to interpret. We will most definitely extend our knowledge to a larger variety of formation histories.

One of the major uncertainties in galaxy evolution remains our detailed understanding of how the abundance of heavy elements, or metallicity, in an interstellar medium varies with time, and thus in different generations of stars. In galaxies that are still forming stars today, the end-point of the metallicity evolution can be measured using H II region emission lines (e.g. Matteucci & Tosi 1985; Pagel & Tautvaišienė 1998), or supergiant stars (e.g. Venn et al. 2001), but deducing how the metal abundances built up to their present levels requires additional information. We want to be able to measure the evolution of metallicity directly and consistently through time, by looking at the properties of stars of different ages. Using a CMD of individual stars in a galaxy it is possible to select RGB stars with ages in the range 1–10 Gyr, and by determining their individual metallicities we can monitor the metallicity evolution of the whole galaxy over this time-frame using the same index. If we then add this independent metallicity information about individual stars to the CMD analysis, we can better disentangle the effects of age and metallicity and determine a more accurate star formation history over the age range 1–10 Gyr (e.g. Brown & Wallerstein 1993; Cole et al. 2000; Hughes & Wallerstein 2000).

The Ca II triplet lines, at 8498, 8542 and 8662 Å, are conveniently among the strongest features in the near-infrared spectra of most late-type stars, and only moderate spectral resolution is required to measure their strengths accurately. The use of the Ca II triplet as a metallicity indicator has a long and checkered history, but after some initial uncertainty it was shown, in the integrated light of a sample of globular clusters, that the Ca II triplet summed equivalent width is strongly affected by metallicity (e.g. Armandroff & Zinn 1988). Subsequent studies backed up this result from measurements of individual globular cluster RGB stars (e.g. Olszewski et al. 1991). An empirical method of ranking globular clusters according to metallicity was first detailed by Armandroff & Da Costa (1991, hereafter AD91), and their basic approach is what has been most generally adopted and refined since then. Rutledge et al. (1997a, hereafter R97a) have presented the most extensive catalogue of Ca II triplet measurements, which Rutledge, Hesser & Stetson (1997b, hereafter R97b) have used to calibrate the Ca II triplet, [Ca/H], to the [Fe/H] scale determined from detailed high-resolution spectroscopy by Zinn & West (1984) and Carretta & Gratton (1997). R97b have shown that the Ca II triplet method is accurate and linear between [Fe/H] = −2.2 and −0.6, which is the range of metallicities that we might expect for the galaxies in our sample.

Thus measuring the summed strengths of the two strongest Ca II triplet lines in the spectra of individual RGB stars and converting, them into a measure of stellar iron abundance is an empirically proven 'quick and dirty;' alternative to high-resolution detailed direct abundance determinations of numerous elements (e.g. AD91; Suntzeff et al. 1993; R97b; Da Costa & Hatzidimitriou 1998; Cole et al. 2000), if we can assume that globular clusters and galaxy field stars will have similar abundance patterns (Smecker-Hane & McWilliam 1999; Shetrone, Côté & Sargent 2001).

With Focal Reducer/low dispersion spectrograph (FORS1) in multi-object spectroscopy (MOS) mode we can efficiently build up a large sample of Ca II triplet measurements of individual stars in nearby galaxies. Using the Ca II triplet lines we can also determine the radial velocity of each star and thus assess the likelihood of membership in the galaxy, and obtain a rough determination of the velocity dispersion of the observed stars within these galaxies.

We chose to observe three nearby galaxies which are known to have complex, long-lasting star formation histories. The resulting large range in age of stars on the RGB makes it very complicated to interpret its properties directly in terms of age or metallicity. The three nearby galaxies chosen are Sculptor dSph, Fornax dSph and NGC 6822 dI (see Table 1). These galaxies have accurate CMDs and quite complex, but relatively well-determined, star formation histories (e.g. Gallart, Aparicio & Vílchez 1996a; Monkiewicz et al. 1999; Buonanno et al. 1999). Stars in four relatively nearby star clusters with well-determined metal abundances and previous Ca II triplet observations were also observed (see Table 2) to calibrate the variation of the Ca II triplet lines as a function of metallicity, and thus tie our results on to the metallicity scale of R97b.

Table 3. The observations.

Date	Begin *UT*	Object	Exp time (s)	Airmass	DIMM* (arcsec)	Effective† (arcsec)	Comments
18Aug99	06:03	Scl-centre	30	1.11	0.5		pre-image
	08:26	Scl-c1	2×1000	1.04	0.7	0.58	
	09:15	Scl-c2	2×1200	1.11	0.85	0.62	
18Aug99	06:07	Scl-out2	30	1.11	0.5		pre-image
19Aug99	06:46	Scl-o2	1200	1.05	0.9	0.7	
	07:11		1000	1.02	0.8		
	07:35		1200	1.01	0.7		
18Aug99	06:11	Scl-out1	30	1.10	0.6		pre-image
19Aug99	08:57	Scl-o1	2×2000	1.12	0.7	0.6	
18Aug99	10:02	Fnx-centre	60	1.02	0.8		pre-image
20Aug99	06:04	Fnx-c1	2×2000	1.2	0.6	0.64	
	08:49	Fnx-c2	2×2000	1.02	0.9	0.68	
18Aug99	05:56	N6822-centre	60	1.46	0.6		pre-image
	01:57	N6822-susi1	3×2000	1.03	0.5	0.56	
19Aug99	02:43	N6822-susi2	3×2000	1.08	0.65	0.6	
20Aug99	00:05	N6822-susi1b	3×2000	1.08	0.6	0.8	
17Aug99	23:35	Rup 106	2×300	1.68	0.7	1.08	
19Aug99	04:44	M 15	2×120	1.26	0.44	0.5	
19Aug99	08:11	47 Tuc-l5406	150	1.49	0.9	1.0	
	08:32	47 Tuc-l3512	2×200	1.50	0.7	0.84	
20Aug99	03:43	Pal 12	2×300	1.02	0.5	0.54	

*This is just an indication of the external seeing measured automatically by the seeing monitor (DIMM) on the mountain. Usually the seeing on the instrument is better than this.
†This is the effective seeing measured from the spatial extent of the spectra on the *combined* images.

2 OBSERVATIONS

The observations were obtained in visitor-mode, with UT1/FORS1 with MOS instrumental set-up, between 1999 August 17 and 20 (see Table 3). At our resolution, the FORS1 MOS field of view is 6.8 arcmin long and ∼2 arcmin wide to cover the full wavelength range (7000–9000 Å). It is covered by 19 mechanical slit jaws which can be moved around the field horizontally for a given orientation on the sky. The slit jaws come from either side of the field to meet at the determined slit width. The length of each slit is fixed, and in the configuration we used each slit is about 20 arcsec long (projected on the sky).

Throughout our observations we used a slit width of 1 arcsec and the GRIS−600I+15 grism along with the OG590 order-sorting filter, to cover the Ca II triplet wavelength region with as high a resolution as possible. With this setting the pixel sampling is close to 1 Å per pixel and the resolution ≈ 2–3 Å over the wavelength range 7050–9150 Å. This is the maximum resolution that can be obtained with FORS1 without resorting to a narrower slit. Although this is a wavelength range at which the FORS1 CCD (Tektronix) has reduced sensitivity, it is where the RGB stars that we were aiming to detect are brightest. The Ca II triplet is also a useful unblended feature to measure radial velocities accurately (e.g. Hargreaves et al. 1994), and there are abundant narrow sky lines in this region for wavelength calibration and/or spectrograph flexure monitoring. The spectrum in the region of the Ca II triplet is also very flat and relatively free of other lines, permitting unambiguous continuum level determination.

The meteorological conditions during this run were always photometric (see Tolstoy et al. 2000), and the seeing, although very good, typically varied by quite a lot during each of the nights (roughly between 0.3 and 0.9 arcsec on the seeing monitor) These data were taken while Paranal was still under construction, before the re-coating of the primary mirror, and were therefore 30–40 per cent below the optimal sensitivity.

The target RGB stars were selected from earlier ESO New Technology Telescope (NTT) imaging in *V* and *I* filters of these galaxies (Tolstoy et al., in preparation). We selected stars from three different fields in Sculptor (see Fig. 1) and one each in Fornax (Fig. 2) and in NGC 6822 (Fig. 3). The selection criteria covered a range in magnitude, and we attempted to get as large as possible a spread in colour across the RGB (see Figs 4, 5 and 6). We also tried to avoid including asymptotic giant branch stars by avoiding the tip region of the RGB, although it has recently been shown (Cole et al. 2000) that this does not have an important impact on the results. Our selection within these criteria was then driven by how best to align the FORS1 MOS field with the available candidates.

Astrometry of the selected targets was determined through the NTT images in combination with the FORS1 pre-imaging. Through-slit images were used to check the crucial centring of objects in their slits. We have been able to use these images to check further for small offsets from centre for the final positions of all the objects over the field. This is crucial to determine accurately radial velocities of all the stars across the MOS field. A shift of 1 pixel of the object from the centre of a 5-pixel-wide slit translates into a $\sim$35 km s^{-1} error in a radial velocity determination. As we show later in this paper, we were able to correct for the small offsets that are inevitable with this kind of complex multi-slit set-up. We also used the through-slit image to correct for uncertain photometry for some of the globular cluster stars.

Membership of each individual star observed in each of the galaxies was assumed based upon their photometric positions in a

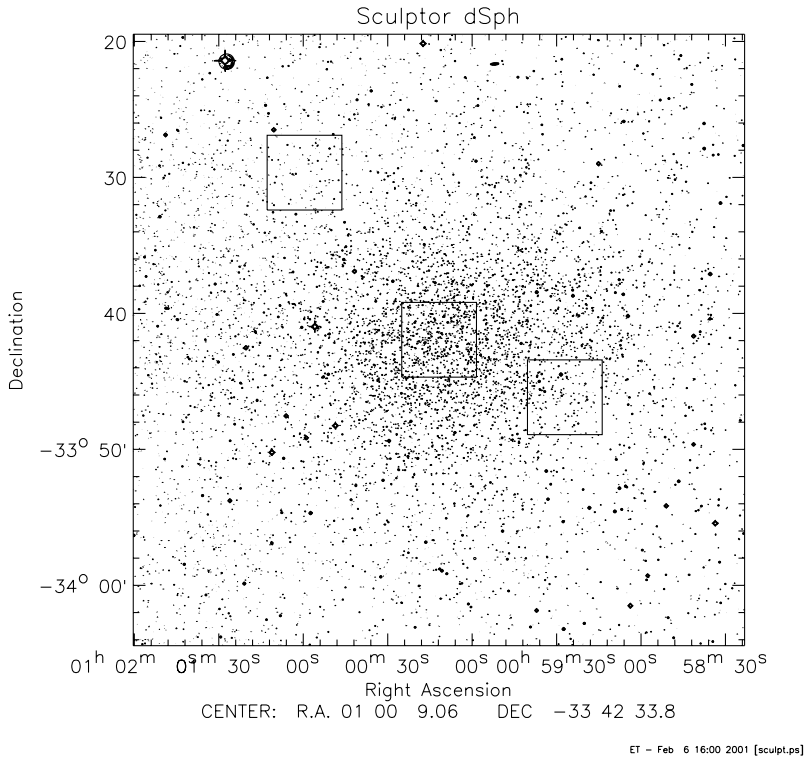

Figure 1. A contour plot 45 arcmin on a side of the Sculptor dSph galaxy, taken from the Palomar Sky Survey. North is up and east is left. The three 5 arcmin square fields for which we have NTT imaging, and thus from where we have selected individual RGB stars, are shown. This image comes from data copyrighted by the Space Telescope Science Institute (STScI Digitized Sky Survey, © 1993, 1994, AURA, Inc. All rights reserved).

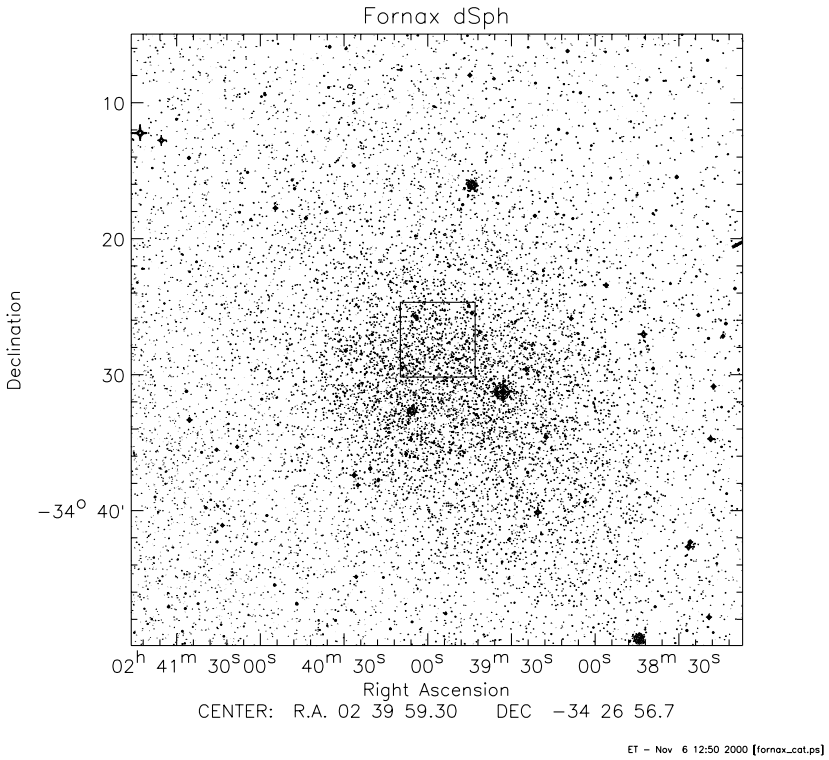

Figure 2. A contour plot 45 arcmin on a side of the Fornax dSph galaxy, as Fig. 1.

CMD. This was then verified from radial velocity determinations based upon the resulting spectra. Happily, there was little evidence for contamination by foreground (or background!) objects in either Sculptor or Fornax, or, within the large uncertainties, in NGC 6822.

3 DATA REDUCTION AND ANALYSIS

As part of standard observing practice on Paranal, bias frames are taken every day, as are internal flat-fields and wavelength

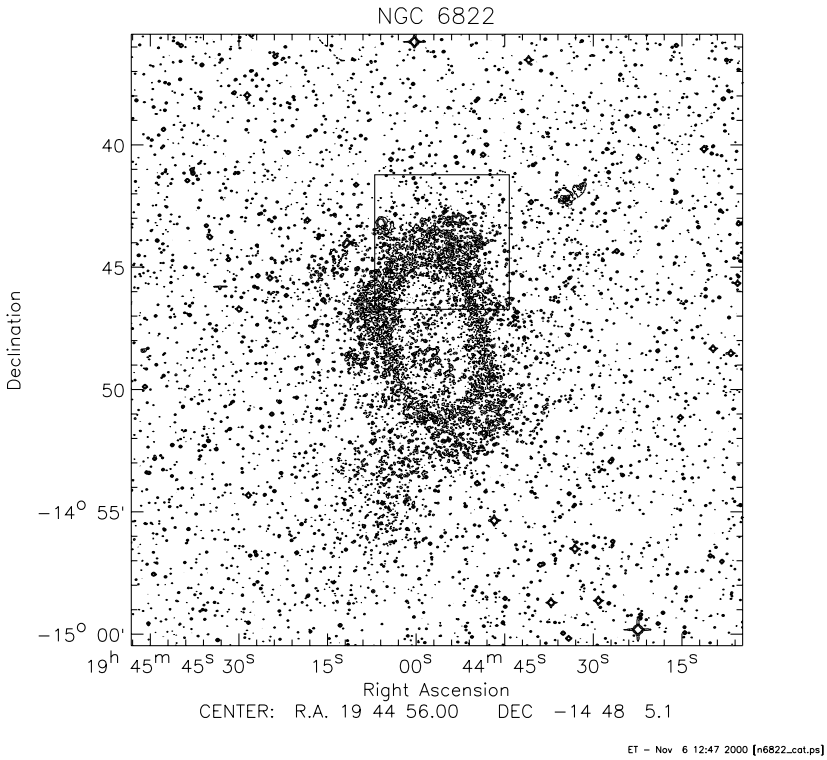

Figure 3. A contour plot 25 arcmin on a side of the NGC 6822 dwarf irregular galaxy, as Fig. 1.

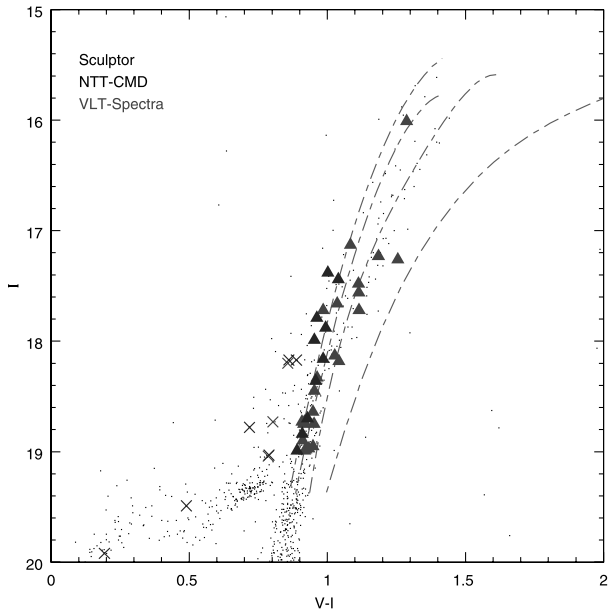

Figure 4. The combined NTT CMD of the stars in all three of the Sculptor fields shown in Fig. 1. Over-plotted as filled triangles are the member stars for which we have FORS1 Ca II triplet spectroscopy. The crosses denote stars for which we have spectroscopy, but either they are not radial velocity members, or the measurements were not usable for one reason or another (see Table 5). The dashed lines are the RGB fiducials for the globular clusters 47 Tucanae, NGC 6752, NGC 6397 and M15 from Da Costa & Armandroff (1990), with metallicities [Fe/H] = −0.7, −1.5, −1.9 and −2.2, from right to left.

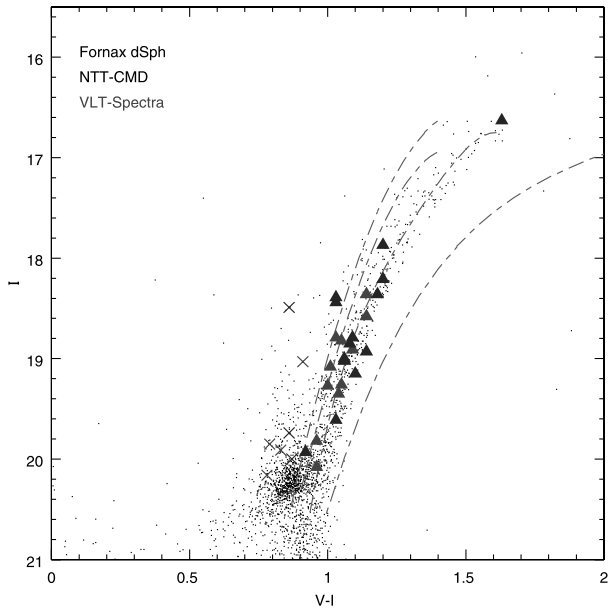

Figure 5. The NTT CMD of the stars in the Fornax field shown in Fig. 2. Over-plotted as filled triangles are the member stars for which we have FORS1 Ca II triplet spectroscopy. The crosses denote stars for which we have spectroscopy, but either they are not radial velocity members, or the measurements were not usable for one reason or another (see Table 6). The dashed lines are the RGB fiducials for the globular clusters (see Fig. 4).

calibration arc spectra, which are taken through the MOS set-ups used at night.

We reduced all our data in IRAF, using standard routines from the CCDRED and APALL packages. We de-biased our frames by making use of the overscan region, and flat-fielded them from the daytime calibration flat-field frames.

Working in the wavelength range 7050–9150 Å at a resolution of 1 Å pixel^{-1}, the night sky lines are plentiful and well distributed over the wavelength range and were used to map the wavelength distortion directly and calibrate the spectra accurately. The adopted reference wavelengths were taken from the on-line Keck LRIS

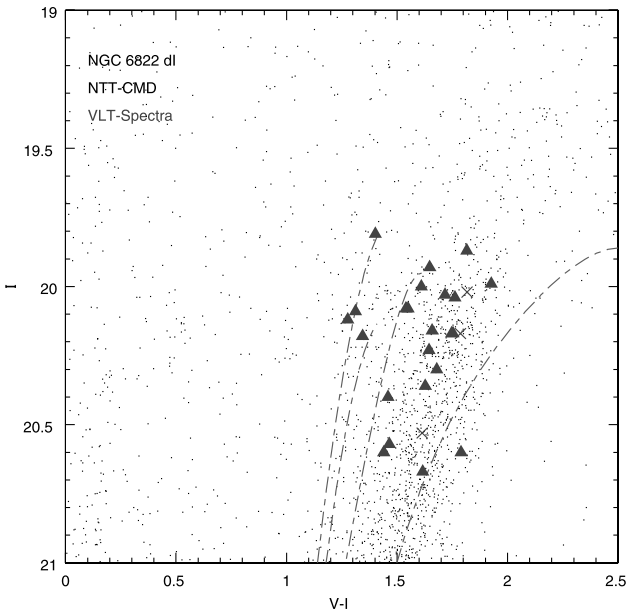

Figure 6. The NTT CMD of the stars in the NGC 6822 field shown in Fig. 3. Over-plotted as filled triangles are the stars for which we have FORS1 Ca II triplet spectroscopy, and which we believe to be members based on the radial velocities. The crosses denote stars that are not likely to be radial velocity members (see Table 7). The dashed lines are the RGB fiducials for the globular clusters (see Fig. 4).

skyline plots, which were in turn based on a compilation by Osterbrock & Martel (1992). This was found to be more accurate than using the daytime arc spectra. The sky was estimated from regions as symmetrically located as possible either side of the target in the (typically) 20 arcsec long slits. The resolution of the spectrograph is 2–3 pixels in the spectral direction and 0.2 arcsec pixel^{-1} in the spatial direction, therefore sky subtraction presents no problem.

3.1 Determining membership: radial velocities

We determined the radial velocities of all the observed stars using the techniques previously described in Tolstoy & Irwin (2000). We created a radial velocity template from Ruprecht 106 – star 1614, which has a previous accurate radial velocity measured by Da Costa, Armandroff & Norris (1992) to be $-54\,\mathrm{km\,s^{-1}}$. This was used as the zero-point comparison for all the radial velocities quoted in this paper, cross-correlating this template with all the other spectra using FXCOR. We further checked the velocity system using the four stars in Pal 12 with previously measured radial velocities (see Table 4).

One of the largest errors in determining radial velocities with this MOS set-up comes from errors in centring the images in the slits. These systematic radial velocity errors can be corrected by determining the offsets of the star position in a through-slit image, and comparing this with a cross-correlation with the position of the telluric A band in their respective spectra to confirm the displacement and correct the wavelength scale appropriately.

Table 4. Calibrator results.

Star	V	$B-V$	$\Sigma W_{\rm ob}$	$v_{\rm r}$(ob) (km s^{-1})	off (km s^{-1})	$v_{\rm r}$(c) (km s^{-1})	$v_{\rm r}$(pr) (km s^{-1})	Ref.
47tuc-l3512	11.8	1.63	6.04 ± 0.05	-47.2 ± 1.6	+20	−27.2	−21	1
47tuc-l5406	12.8	1.30	5.41 ± 0.13	-48.8 ± 1.8	+21	−27.8	−29	1
m15-38	14.4	0.97	2.09 ± 0.10	-33.4 ± 2.8	−82	−115.4		2
m15-24	13.6	1.14	2.56 ± 0.14	-39.6 ± 2.5	−39	−79.0		2
m15-58†	16.1	0.77	2.57 ± 0.13	-50.3 ± 4.2	−58	−108.3		2
m15-195†	16.4	0.72	2.44 ± 0.45	-44.1 ± 7.4	−62	−103.1		2
m15-260	14.5	0.97	2.22 ± 0.15	-40.6 ± 2.1	−69	−109.6		2
m15-302‖	14.2	0.99	2.78 ± 0.33	-69.1 ± 3.8	−31	−100.1		2
m15-371	13.6*	0.91	2.27 ± 0.25	-39.5 ± 3.9	−74	−113.5		2
m15-459	14.4*	0.80	2.16 ± 0.11	-43.9 ± 2.7	−37	−79.7		2
m15-462	13.1*	0.99	2.97 ± 0.23	-28.5 ± 2.6	−78	−106.4		2
pal12-3111‖	17.16	0.76	4.89 ± 0.42	-24.3 ± 4.2	+39	14.7		3
pal12-S1	14.58	1.58	6.45 ± 0.11	-21.7 ± 2.6	+68	46.3	30.6	3,4,5
pal12-3460	16.69	0.83	4.77 ± 0.18	4.7 ± 1.7	+10	14.7		3
pal12-1118	14.79	1.52	6.26 ± 0.07	-13.5 ± 1.9	+21	7.5	25.3	3,4,5
pal12-1128	15.35	1.26	5.50 ± 0.09	65.8 ± 1.7	−60	5.8	27.1	3,4
pal12-1329	17.06	0.79	4.32 ± 0.22	26.8 ± 1.9	+12	38.8		3
pal12-1305	15.86	1.10	5.39 ± 0.12	-4.7 ± 1.4	+33	28.3	30.9	3,4
pal12-3328	17.17	0.74	4.27 ± 0.16	44.3 ± 1.8	−33	11.3		3
rup106-1730†	14.8	0.65	3.86 ± 0.10	13.2 ± 2.2	−30	−16.8		6
rup106-1614‡	14.7	1.67	4.74 ± 0.05	-53.5 ± 1.5			−54	5,6,7
rup106-1067†	13.5	0.91	5.60 ± 0.09	66.5 ± 2.1	−62	+4.5		6
rup106-1092	13.9	1.27	5.44 ± 0.05	-86.2 ± 1.9	−4	−90.2		6
rup106-580	14.1*	1.17	5.28 ± 0.07	-15.3 ± 1.4	−51	−66.3		6
rup106-236	14.3*	1.58	5.04 ± 0.05	54.9 ± 2.1	−57	−2.1		6

Notes. †Not an RGB star; not included in Fig. 11.
‖Large error bars; not included in Fig. 11.
*Photometry corrected for relative flux in the through-slit image.
‡Defined as a radial velocity standard. Sources of photometry, star identification and previous radial velocity measurements: (1) Da Costa & Armandroff (1986); (2) Buonanno et al. (1983); (3) Harris & Canterna (1980); (4) AD91; (5) Brown, Wallestein & Zucker 1997; (6) Buonanno et al. (1990); (7) Da Costa et al. (1992).

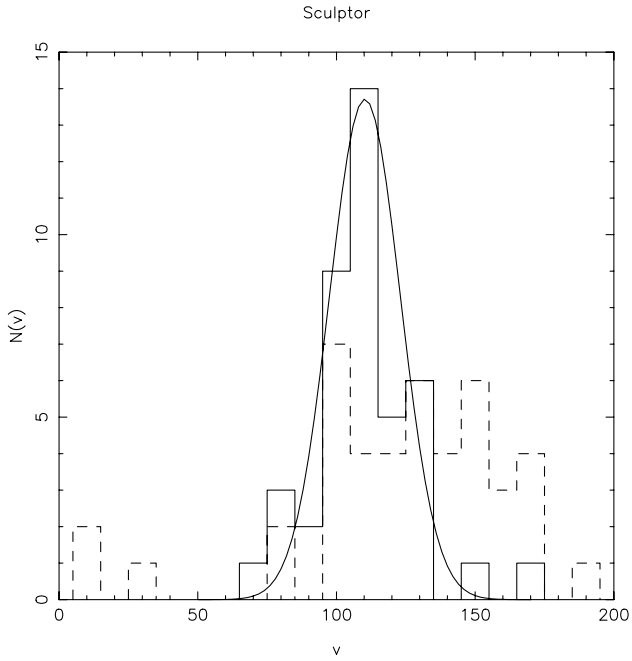

Figure 7. A histogram of the radial velocity determinations for the spectroscopically observed stars in Sculptor dSph (as shown in Fig. 4). The dashed line represents the distribution of directly measured radial velocities, and the solid line is the distribution after corrections have been made for the position of each object in the slit, with a Gaussian fit to these corrected points. The central velocity that we found here is $110.2\,\mathrm{km\,s^{-1}}$, with a dispersion $\sigma_v = 12.8$, which compares to the literature values of $110\,\mathrm{km\,s^{-1}}$ and $\sigma_v = 6$ (Armandroff & Da Costa 1986; Queloz et al. 1995), giving a resulting accuracy of our velocity measurements of $\pm 10.7\,\mathrm{km\,s^{-1}}$.

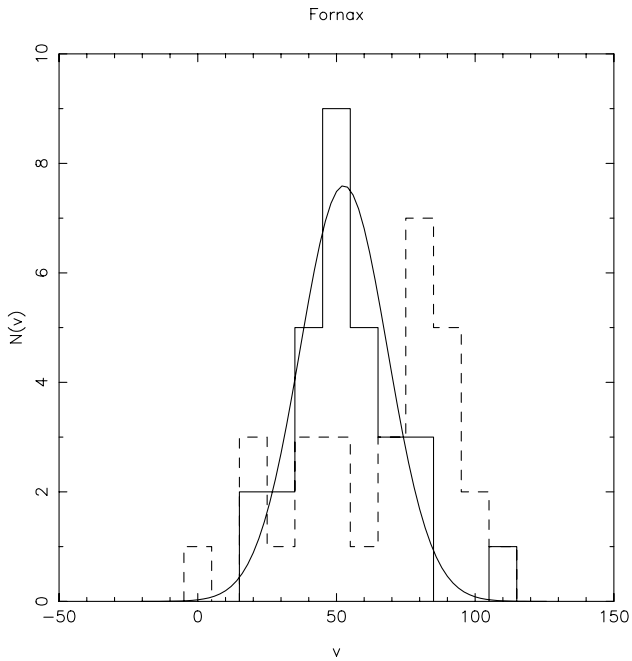

Figure 8. A histogram of the radial velocity determinations for the spectroscopically observed stars in Fornax dSph (as shown in Fig. 5). The different lines are as described in Fig. 7. The central velocity that we found here is $52.7\,\mathrm{km\,s^{-1}}$, with a dispersion $\sigma_v = 15.8$, which compares to the literature values of $53\,\mathrm{km\,s^{-1}}$ and $\sigma_v = 11$ (Mateo et al. 1991), giving a resulting accuracy of our velocity measurements of $\pm 11.3\,\mathrm{km\,s^{-1}}$.

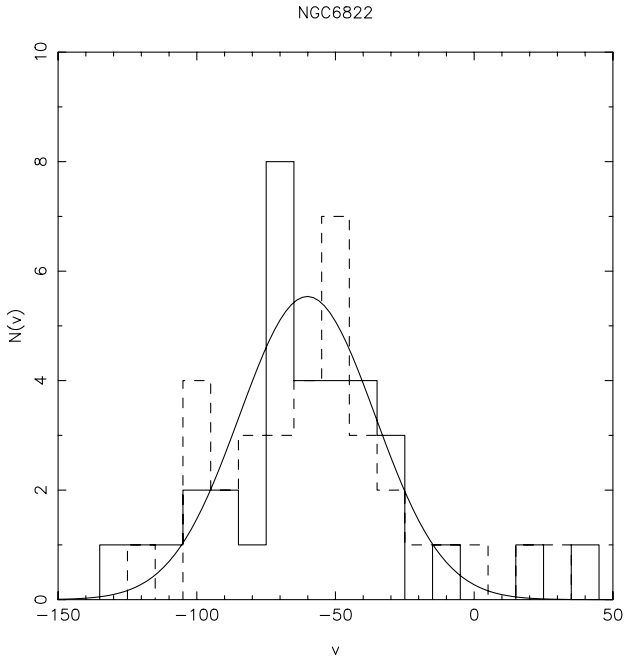

Figure 9. A histogram of the radial velocity determinations for the spectroscopically observed stars in NGC 6822 dI (as shown in Fig. 6). The different lines are as described in Fig. 7. The central velocity that we found here is $-60.1\,\mathrm{km\,s^{-1}}$, with a dispersion $\sigma_v = 24.5$, which compares to the literature value of $-57\,\mathrm{km\,s^{-1}}$ for the central velocity (Richter et al. 1987). The equivalent global velocity dispersion for NGC 6822 from H I measurements is $34\,\mathrm{km\,s^{-1}}$.

As shown in Figs 7, 8 and 9 for each galaxy, the histogram of radial velocity tightens up significantly about the (known) radial velocity of the galaxy after the correction has been applied. The expected stellar velocity dispersion within globular clusters and dwarf spheroidals is known to be about $\pm 10\,\mathrm{km\,s^{-1}}$ (e.g. Harris 1996; Mateo 1998), but within larger dI galaxies this is not so well known, and is also much less meaningful, as dIs typically rotate. In H I gas NGC 6822 has a velocity difference of $100\,\mathrm{km\,s^{-1}}$ from one side to the other (Brandenburg & Skillman 1998; de Blok & Walter 2000), and the velocity dispersion that we see in Fig. 9 is a combination of the effects of differential rotation over the field and random motion.

Radial velocities were derived for all the spectra mainly for use in determining membership probabilities. Rather than using radial velocity standards, we calibrated our velocity system using the known radial velocities of stars within globular clusters that we also observed. This also has the added advantage of providing a better template match for cross-correlation. The majority of the RGB-selected stars in each MOS field ought to be members of the galaxies because of the careful photometric selection. In combination with the radial velocity information, this generally leads to unambiguous membership assignment. For Fornax and Sculptor, previous studies at high resolution have shown the dispersion to be around $10\,\mathrm{km\,s^{-1}}$ (Armandroff & Da Costa 1986; Queloz et al. 1995; Mateo et al. 1991). Based upon the dispersion that we measure from our spectra, we determine our criteria for membership such that within 3σ of the central velocity is a 'definite' member, and in the range 3σ–5σ is a 'maybe', and those (very few) outside this range are highly unlikely to be members of the system.

In the cases of Fornax and NGC 6822 there is likely to be a degree of foreground Galactic star contamination which cannot be

eliminated by radial velocity information. The velocity of Fornax is very low, and thus it is frequently hard to distinguish members of Fornax dSph from stars in our Galaxy (see Mateo et al. 1991), but careful colour selection helps to minimize this contamination. Fornax is at high Galactic latitude, so this effect is in any case likely to be small, but NGC 6822 has both a low velocity and a low Galactic latitude. It is liable to have significant contamination which we will be unable to detect directly (see also Gallart et al. 1996a). This can clearly be seen in our NGC 6822 CMD (in Fig. 6): compared with Fornax (Fig. 5) and Sculptor (Fig. 4), there are obviously field stars over the entire area of the NGC 6822 RGB. This is seen as a scatter of points covering the magnitude and colour range plotted in Fig. 6. NGC 6822 also suffers from significant reddening without much information on the differential effects. None the less, the distribution of velocities of the RGB stars selected in NGC 6822 is still peaked about the expected value of the galaxy (from Richter, Tammann & Huchtmeier 1987), and so this gives us confidence that the contamination is likely to be a small fraction of the total.

3.2 Determining the abundance: equivalent widths

We measured equivalent widths of the Ca II triplet lines in IRAF by fitting a Gaussian profile to each line and determining the continuum consistently on either side of the line. The weakest Ca II line at 8498 Å was not used in any analysis. It is often of very low signal-to-noise ratio, especially at low metallicity, and is more affected by sky lines than the other two. The error estimates on the Gaussian fits as provided by the fitting routine are given in Tables 4–7. The errors in the equivalent width owing to inaccurate continuum placement in the Ca II triplet region are much less than the random errors. We also checked for a possible offset caused by

Table 5. Sculptor results.

Star	I	$V-I$	$W_{8542}+W_{8662}$	[Fe/H]	v_r(meas) (km s^{-1})	offset (km s^{-1})	v_r(corr) (km s^{-1})
c1-56*	18.2	0.86	3.35 ± 0.24		130.6 ± 2.4	−2	128.6
c1-70	17.7	1.12	4.26 ± 0.24	−1.28 ± 0.10	101.2 ± 2.2	+26	127.2
c1-85	18.6	0.95	3.73 ± 0.46	−1.30 ± 0.19	75.9 ± 2.9	+13	88.9
c1-68	19.0	0.92	3.07 ± 0.43	−1.49 ± 0.18	113.2 ± 3.2	+6	119.2
c1-101	17.7	1.04	3.21 ± 0.20	−1.76 ± 0.08	95.4 ± 1.9	+15	110.4
c1-99§	18.2	1.00	4.54 ± 0.27		133.3 ± 1.9	+73	206.3
c1-43	18.3	0.96	3.29 ± 0.48	−1.56 ± 0.20	162.3 ± 3.9	−54	108.3
c1-55*	18.7	0.80	3.29 ± 0.71		146.7 ± 4.0	−43	103.7
c1-67¶	19.0	0.79	3.69 ± 0.89		170.2 ± 4.3	−16	154.2
c1-76	18.5	0.95	3.60 ± 0.43	−1.40 ± 0.18	122.5 ± 3.8	−10	112.5
c1-81	16.0	1.29	2.98 ± 0.11	−2.23 ± 0.05	101.3 ± 1.5	−31	70.3
c1-46	17.6	1.11	4.60 ± 0.52	−1.18 ± 0.22	193.7 ± 4.9	−108	85.7
c1-47	17.7	0.99	3.88 ± 0.22	−1.47 ± 0.09	107.0 ± 2.2	+4	111.0
c1-88	17.5	1.11	4.40 ± 0.23	−1.28 ± 0.10	75.7 ± 2.8	+35	110.7
c1-78	17.2	1.19	3.98 ± 0.19	−1.51 ± 0.08	105.3 ± 2.8	+7	112.3
c2-64	17.1	1.08	3.27 ± 0.16	−1.87 ± 0.07	133.9 ± 1.7	−32	101.9
c2-81	18.1	1.03	4.10 ± 0.30	−1.27 ± 0.13	152.5 ± 2.3	−23	129.5
c2-88	18.7	0.92	3.61 ± 0.48	−1.34 ± 0.20	104.1 ± 4.4	+3	107.1
c2-73*	18.2	0.92	2.90 ± 0.44		103.8 ± 4.5	0.	103.8
c2-38	18.9	0.91	2.99 ± 0.61	−1.56 ± 0.26	125.2 ± 4.2	−29	96.2
c2-39*	18.2	0.89	2.53 ± 0.33		134.8 ± 4.9	−11	123.8
c2-72	18.7	0.91	3.27 ± 0.62	−1.49 ± 0.26	95.5 ± 4.2	−20	75.5
c2-52	18.8	0.91	3.44 ± 0.74	−1.41 ± 0.31	142.2 ± 5.2	−44	98.2
c2-27	19.0	0.95	4.71 ± 0.63	−0.81 ± 0.27	115.6 ± 7.0	−34	81.6
c2-60	19.0	0.93	3.97 ± 0.71	−1.12 ± 0.30	159.1 ± 4.4	−49	110.1
c2-86	18.8	0.95	4.36 ± 0.75	−1.01 ± 0.32	158.0 ± 4.9	−41	117.0
c2-82	18.2	1.04	3.08 ± 0.34	−1.68 ± 0.14	168.8 ± 3.5	−58	110.8
c2-53	19.0	0.92	3.67 ± 0.65	−1.25 ± 0.27	135.0 ± 5.5	−54	81.0
c2-85	17.3	1.26	3.99 ± 0.18	−1.49 ± 0.08	165.3 ± 1.5	−63	102.3
o1-1	17.8	0.96	1.92 ± 0.15	−2.30 ± 0.05	122.6 ± 2.8	−3	119.6
o1-4	17.4	1.04	4.56 ± 0.18	−1.27 ± 0.05	114.9 ± 2.0	−7	107.9
o1-11*	19.0	0.79	3.57 ± 0.46		77.5 ± 4.1	+32	109.5
o1-14¶	19.5	0.49	3.41 ± 0.75		138.6 ± 4.6	−9	129.6
o1-6	18.2	0.99	3.76 ± 0.20	−1.42 ± 0.08	98.9 ± 2.1	+2	100.9
o1-15§	19.9	0.19	6.32 ± 0.97		173.9 ± 6.1	−6	167.9
o1-21	17.4	1.00	3.01 ± 0.22	−1.94 ± 0.09	121.4 ± 1.9	−17	104.4
o1-22	18.8	0.91	2.24 ± 0.29	−1.90 ± 0.12	153.4 ± 7.6	−39	114.4
o1-30†	17.9	2.33	2.36 ± 0.15		14.0 ± 4.2	−32	−18.
o2-28*	18.8	0.72	1.69 ± 0.81		151.1 ± 6.7	−38	113.1
o2-25	18.0	0.95	3.80 ± 0.39	−1.43 ± 0.16	150.9 ± 3.1	−43	107.3
o2-33	19.0	0.89	2.80 ± 0.76	−1.60 ± 0.32	142.3 ± 3.3	−8	134.3
o2-38	18.7	0.93	3.86 ± 0.57	−1.23 ± 0.24	125.6 ± 2.8	−10	115.6
o2-46	18.4	0.96	2.90 ± 0.53	−1.71 ± 0.22	141.5 ± 3.1	−14	127.5
o2-44	17.9	0.99	3.83 ± 0.34	−1.44 ± 0.14	145.2 ± 4.2	−43	102.2

§Probably not a Sculptor member, from radial velocity; not included in Fig. 12.
¶Probably a horizontal branch star in Sculptor; not included in Fig. 12.
*Too blue to be an RGB star; not included in Fig. 12.
† This could be a Galactic M star, certainly not a Sculptor member; not included in Fig. 12.

Table 6. Fornax results.

Star	I	$V-I$	$W_{8542}+W_{8662}$	[Fe/H]	v_r(meas) (km s^{-1})	offset (km s^{-1})	v_r(corr) (km s^{-1})
c1-660*	19.0	0.91	6.94 ± 0.09		88.7 ± 1.7	−41	47.7
c1-350‖	19.9	0.83	4.63 ± 0.97	−0.92 ± 0.41	75.9 ± 4.6	−13	62.9
c1-444	19.3	1.04	5.55 ± 0.64	−0.63 ± 0.31	94.1 ± 3.2	−23	71.1
c1-371	18.9	1.09	4.41 ± 0.33	−1.21 ± 0.17	84.0 ± 2.3	−30	54.0
c1-601	18.8	1.03	6.22 ± 0.26	−0.50 ± 0.15	81.3 ± 3.0	−32	49.3
c1-628	19.3	1.00	5.52 ± 0.52	−0.67 ± 0.29	99.7 ± 2.7	−49	50.7
c1-564	19.3	1.05	4.46 ± 0.40	−1.11 ± 0.25	79.6 ± 4.5	−29	50.6
c1-433*	20.2	0.78	4.55 ± 1.10		94.6 ± 10.6	−34	60.6
c1-365*	19.8	0.79	6.01 ± 0.83		81.1 ± 4.0	−28	53.1
c1-122‖	20.1	0.96	5.15 ± 0.89	−0.62 ± 0.37	104.8 ± 7.7	−49	55.8
c1-125‖	19.8	0.96	6.35 ± 1.40	−0.19 ± 0.59	90.3 ± 4.5	−48	42.3
c1-214	18.4	1.14	4.64 ± 0.33	−1.25 ± 0.14	92.2 ± 2.8	−40	52.2
c1-360	18.6	1.14	5.85 ± 0.23	−0.68 ± 0.14	65.3 ± 2.6	0.	65.3
c1-200	18.8	1.05	4.58 ± 0.31	−1.18 ± 0.19	107.1 ± 3.0	−25	82.1
c1-344	19.1	1.01	4.52 ± 0.68	−1.14 ± 0.27	89.3 ± 5.4	−36	53.3
c2-822	19.6	1.03	5.43 ± 0.58	−0.61 ± 0.35	82.9 ± 3.5	−21	61.9
c2-777	19.0	1.06	4.27 ± 0.44	−1.25 ± 0.21	43.4 ± 3.4	0.	43.4
c2-838	16.6	1.63	5.39 ± 0.09	−1.27 ± 0.02	1.6 ± 2.6	+40	41.6
c2-828	17.9	1.20	3.98 ± 0.18	−1.64 ± 0.07	72.0 ± 1.9	−6	66.0
c2-702	18.4	1.03	5.68 ± 0.26	−0.83 ± 0.12	64.5 ± 2.4	0.	64.5
c2-613	18.9	1.08	6.02 ± 0.48	−0.55 ± 0.20	19.5 ± 2.0	+13	32.5
c2-769	18.2	1.20	5.55 ± 0.20	−0.89 ± 0.10	42.5 ± 2.5	+8	50.5
c2-511*	18.5	0.86	5.18 ± 0.25		47.6 ± 2.0	+23	70.6
c2-623	18.9	1.14	4.85 ± 0.36	−1.01 ± 0.18	66.0 ± 2.9	−6	60.0
c2-388	19.2	1.10	4.95 ± 0.46	−0.92 ± 0.30	52.7 ± 2.9	−12	40.7
c2-384‖	19.9	0.92	5.26 ± 0.96	−0.63 ± 0.40	58.0 ± 7.7	+2	60.0
c2-294*	20.0	0.87	4.74 ± 1.15		41.1 ± 8.8	+15	56.1
c2-552	18.4	1.03	4.80 ± 0.29	−1.19 ± 0.13	24.7 ± 1.4	−1	23.7
c2-249*	19.7	0.86	5.05 ± 0.93		54.7 ± 5.5	+14	68.7
c2-413	18.4	1.18	5.32 ± 0.20	−0.95 ± 0.14	23.3 ± 2.0	+18	41.3
c2-647	18.8	1.09	4.80 ± 0.30	−1.08 ± 0.20	29.8 ± 1.8	+4	33.8
c2-621	19.0	1.06	4.33 ± 0.49	−1.22 ± 0.20	45.0 ± 5.3	+14	59.0
c2-41	19.0	1.06	3.63 ± 0.59	−1.52 ± 0.26	82.6 ± 2.8	0.	82.6

*Too blue to be an RGB star; not included in Fig. 15.
‖Large error bars on equivalent width measurements; plotted as crosses in Fig. 15.

Table 7. NGC 6822 results.

Star	I	$V-I$	$W_{8542}+W_{8662}$	[Fe/H]	v_r(meas) (km s^{-1})	offset (km s^{-1})	v_r(corr) (km s^{-1})
s1-309	20.6	1.77	2.17 ± 0.38	−2.34 ± 0.16	−40.9 ± 10.4	−10	−50.9
s1-186‖	20.6	1.44	5.14 ± 1.23	−1.18 ± 0.52	−47.7 ± 9.6	−6	−53.7
s1-212‖	20.0	1.91	7.19 ± 0.92	−0.36 ± 0.39	−100.4 ± 3.4	+26	−71.4
s1-210	20.1	1.52	5.75 ± 0.71	−1.04 ± 0.59	−90.4 ± 4.1	+17	−73.4
s1-200	20.2	1.64	5.02 ± 0.51	−1.29 ± 0.43	−95.9 ± 4.7	+52	−43.9
s1-59	20.2	1.26	5.03 ± 0.56	−1.40 ± 0.47	−41.2 ± 6.3	+1	−40.2
s1-188	20.5	1.44	6.69 ± 0.78	−0.58 ± 0.65	−45.8 ± 4.4	−7	−52.8
s1-153	20.2	1.73	5.96 ± 0.71	−0.87 ± 0.60	−75.9 ± 3.7	−5	−80.9
s1-43	20.7	1.60	5.97 ± 0.54	−0.77 ± 0.45	−53.3 ± 6.8	+11	−42.3
s1-205§	20.1	1.80	3.26 ± 1.01		+21.7 ± 5.9	+11	+32.7
s1-204‖	20.6	1.45	4.68 ± 1.35	−1.38 ± 0.57	−53.8 ± 6.5	+25	−28.8
s1-378§	20.2	1.77	5.15 ± 0.91		−104.0 ± 5.4	−23	−127.0
s1-111	20.1	1.53	4.81 ± 0.28	−1.43 ± 0.12	+29.8 ± 2.0	−57	−27.2
s1b-280	20.3	1.66	3.66 ± 0.75	−1.82 ± 0.32	+0.7 ± 12.6	−31	−30.3
s2-208	20.4	1.61	7.18 ± 0.96	−0.34 ± 0.40	−82.8 ± 6.2	−4	−86.8
s2-246	19.9	1.80	6.52 ± 0.48	−0.70 ± 0.20	−72.2 ± 4.4	+4	−68.2
s2-263	20.2	1.32	6.09 ± 0.54	−0.92 ± 0.23	−30.3 ± 4.6	0	−30.7
s2-352	20.3	1.62	5.65 ± 0.80	−1.01 ± 0.34	−50.7 ± 4.2	−27	−77.7
s2-354	20.1	1.74	6.62 ± 0.85	−0.63 ± 0.36	−5.7 ± 5.0	−55	−60.7
s2-250	20.1	1.29	6.33 ± 0.68	−0.86 ± 0.29	−60.1 ± 6.2	−25	−85.1
s2-271	20.2	1.73	7.56 ± 0.75	−0.20 ± 0.32	−47.9 ± 6.3	−25	−72.9
s2-142	20.0	1.63	3.71 ± 0.46	−1.91 ± 0.19	−48.6 ± 5.4	−10	−59.6
s2-248	20.1	1.70	6.22 ± 0.83	−0.81 ± 0.35	−40.1 ± 6.5	−25	−65.1
s2-117‖	19.9	1.38	5.60 ± 1.16	−1.21 ± 0.49	−65.7 ± 3.6	+26	−39.7
s2-199§	20.6	1.59	5.09 ± 0.87		−76.0 ± 7.5	−39	−115.0
s2-198	20.1	1.59	6.52 ± 0.47	−0.72 ± 0.20	−17.2 ± 5.3	−38	−55.2

§Probably not a NGC 6822 member, from radial velocity; not included in Fig. 18.
‖Large error bars on equivalent width measurements; error bars not included in Fig. 18.

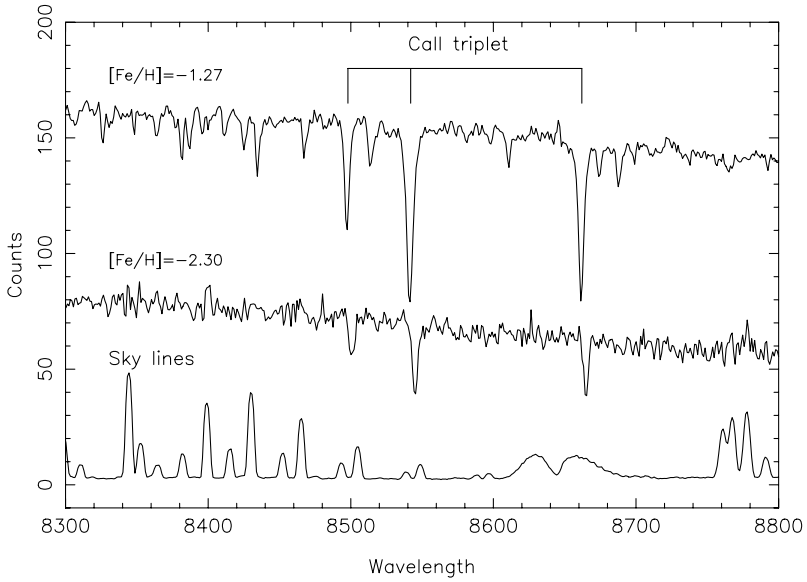

Figure 10. Here we show two examples of spectra at the opposite extremes of our observed Ca II triplet linewidths. For display purposes the spectra have been normalized to their continuum level and then arbitrarily shifted. The upper spectrum is of star c2-838 in Fornax with a calcium triplet metallicity of [Fe/H] = −1.27, and the lower spectrum is of star o1-1 in Sculptor, with [Fe/H] = −2.30. They both have good signal-to-noise ratio, with ∼30 in the upper spectrum and ∼20 in the lower. Also shown here is the sky spectrum. This shows that, although this region of the spectrum is relatively free of bright sky lines, the weaker Ca II triplet line at 8498 Å is more likely to be affected by sky lines than the other two.

the Gaussian fitting function by comparing these results with a simple total integration over the lines, and found negligible (<1 per cent) systematic differences. We present examples of spectra with different linewidths (and thus metallicity) in Fig. 10.

The dependence of the Ca II linewidths on surface gravity, for metallicities below [Ca/H] = −0.3 on the RGB above the horizontal branch, has been shown to be a simple linear relationship between W', which we define as the summed width of λλ8542 and 8662, and the absolute magnitude, M_V, of the star which can be parametrized by $(V - V_{\rm HB})$, the difference in magnitude between the observed RGB star and the level of the horizontal branch (e.g. AD91; R97b). So this dependence can be easily removed, and we are left with a straightforward dependence of W' on metallicity. In common with Cole et al. (2000), we rederived the R97b relation, which requires the minimum of assumptions and input data:

$$W' = \Sigma W(\mathrm{Ca}) + 0.64(\pm 0.02)(V - V_{\rm HB}),$$

where $\Sigma W(\mathrm{Ca}) = W_{8542} + W_{8662}$, which is very similar to the linear regime of the AD91 calibration. We also adopted the abundance scale of Carretta & Gratton (1997), which was shown by R97b to scale linearly with W' as

$$[\mathrm{Fe/H}]_{\rm CG97} = -2.66 + 0.42W'.$$

We rederived this relation using observations of individual stars in globular clusters of known metallicity. We can now apply this abundance scale to our observations of individual stars in nearby galaxies.

There are a number of uncertainties involved in putting the stars observed in galaxies on the same basis as the measurement of globular clusters, as extensively discussed in R97a and Cole et al. (2000). The most important is the [Ca/Fe] ratio, which is likely to vary depending upon the star formation history of the galaxy, and the ratio of old to young stellar populations. The [Fe/H] abundance at a given age should be related to the total amount of past star formation (until that age), but [Ca/Fe] at a given age is a function of the ratio of star formation during the past 100 Myr prior to that age, and the total star formation until that age. This means that care must be taken in converting between Ca and Fe abundances, and a Galactic-halo-like calibration is suitable for those cases when the total star formation is dominated by the very earliest times (e.g. Draco and Ursa Minor: Shetrone et al. 2001), but a Galactic-disc-like calibration is better for a more constant star formation rate (e.g. Smecker-Hane & McWilliam 1999 for the Sagittarius dSph). When a galaxy is dominated by discrete episodes of star formation, especially in recent times, it becomes difficult to determine a unique metallicity scale from a single element abundance (e.g. Pagel & Tautvaišienė 1998, for the Small Magellanic Cloud; Cole et al. 2000).

There is also the problem of choosing the correct value of $V_{\rm HB}$, which varies systematically with age in a galaxy with extended periods of star formation (Cole 1998). In stellar populations much younger than the calibrating globular clusters, the corresponding $V_{\rm HB}$ will likely be brighter than predicted for given metallicity (e.g. Da Costa & Hatzidimitriou 1998). This effect is exacerbated in a system with young stars and variable reddening, such as NGC 6822. For field stars, with an a priori unknown age, we cannot do anything about this fact, which could add a bias of order 0.1 dex to the metallicity of an individual star. However, this does not preclude a detailed analysis of the results, provided that care is taken in the interpretation (Cole et al. 2000).

4 RESULTS

4.1 Calibration globular clusters

To calibrate our observations on to a metallicity scale, as demonstrated in the comprehensive studies of globular clusters by AD91 and R97b, we observed individual stars in four globular clusters: M15, Rup 106, Pal 12 and 47 Tuc, which cover the metallicity range in which we are interested (see Table 2), and which have previously been studied and put into a global scheme by AD91 and R97b. There appear to be inherent differences in the

measurement of equivalent widths between previous studies, probably because of differences in line fitting techniques and telescope and instrument properties (see R97a,b for a detailed discussion), and so we redetermine the scale using our own observations.

The results of our observations of stars in globular clusters are listed in Table 4, which shows: the cluster and star number in column 1; the V magnitude of the star in column 2; the $B - V$ colour in column 3; our measured summed equivalent width of the two strongest Ca II triplet lines, $\Sigma W_{\rm ob} = W_{8542} + W_{8662}$, in column 4; the uncorrected observed radial velocity, $v_{\rm r}$(ob), in column 5; the correction to the observed radial velocity owing to the offset of the star in the slit in column 6; the corrected velocity after this offset has been applied, $V_{\rm r}$(c), in column 7; a previous measurement of the radial velocity of the star if one exists in column 8; and the references for the colour, magnitude and any previous observations for each star in column 9.

In Fig. 11 the summed Ca II equivalent widths are plotted as a function of $V - V_{\rm HB}$ for the stars in our calibration clusters. For each cluster the line of constant metallicity is plotted, using the R97b calibration described in Section 3.2, as a dashed line.

Broadly speaking, our results fit consistently on to the previous abundance scale determined by R97b, even though we define W' differently (R97a use a weighted sum of all three triplet lines). The mean metallicity of Rup 106 is found to be somewhat higher ([Fe/H] $= -1.4$) than that determined by Da Costa et al. (1992) ([Fe/H] $= -1.7$), but it is more consistent with the value measured by Brown et al. (1997) from high-resolution spectroscopy. In the case of M15, we find it to be slightly more metal-rich ([Fe/H] $= -2.15$) than expected from high-resolution spectroscopy, where Sneden et al. (1997) find values around [Fe/H] $= -2.3$. Sneden et al. noted that M15 has an unusually high [Ca/Fe] ratio, which could explain this discrepancy. Pal 12 appears to have a slightly higher mean metallicity ([Fe/H] $= -0.8$) than high-resolution spectroscopy found ([Fe/H] $= -1.0$), from Brown et al. (1997), but consistent with previous Ca II triplet observations (R97a). Our data also support the metallicity spread noted by Brown et al. arising from variations in the [Ca/Fe] ratio within this cluster.

It is known that the [Ca/Fe] ratio is not really that constant over the globular cluster population (Carney 1996). Therefore there is an implicit assumption in the use of the AD91 and R97b calibrations that the objects of interest have experienced a similar evolution of the [Ca/Fe]-to-[Fe/H] ratio to the globular clusters. fig. 8 of Cole et al. (2000) shows how this assumption may break down for the Large Magellanic Cloud, because of its complex star formation history. Until the Ca II triplet equivalent width can be calibrated to a scale that ties it directly to [Ca/H], this remains the ultimate limitation on the accuracy of the method.

4.2 Sculptor dwarf spheroidal

4.2.1 Background

The Sculptor dSph galaxy was discovered by Shapley in 1938 (Shapley 1938), and Baade & Hubble (1939) noted its similarity to a globular cluster, except for size and distance. Sculptor was found to contain a very rich population of RR Lyrae variable stars

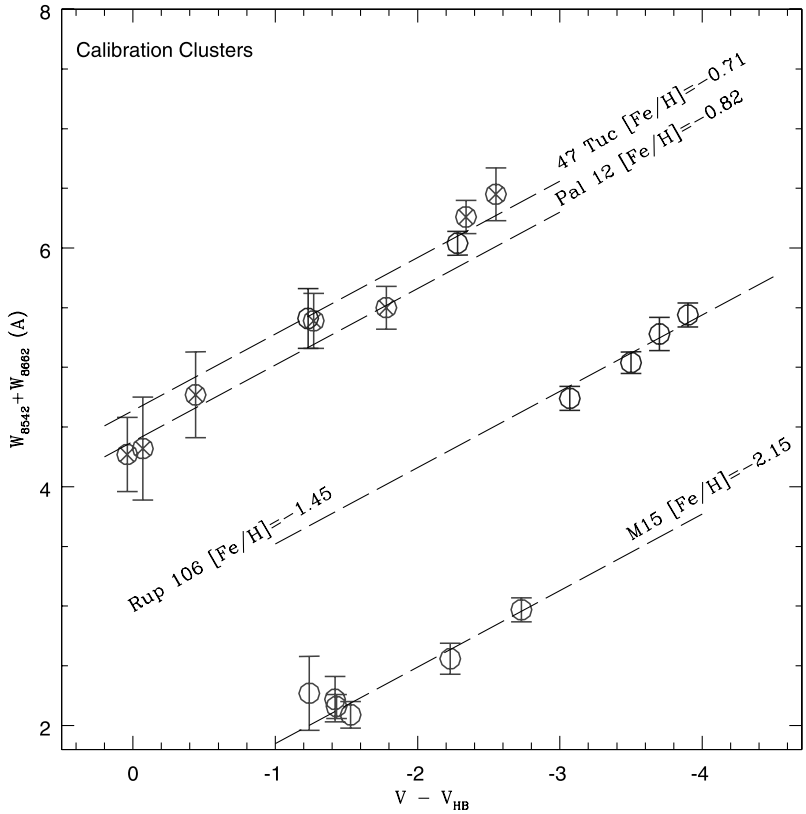

Figure 11. The summed equivalent width of the two stronger Ca II triplet lines ($W_{8542} + W_{8662}$) is plotted against the V magnitude difference from the horizontal branch ($V - V_{\rm HB}$) for the observed stars in the calibration globular clusters Pal 12, 47 Tucanae, Ruprecht 106 and M15. The Pal 12 measurements are plotted as open circles with crosses to distinguish them from the two 47 Tuc measurements (open circles). Also plotted for each cluster are the best-fitting lines, with slope 0.64 (see Section 3.2), and the metallicity to which these correspond is indicated.

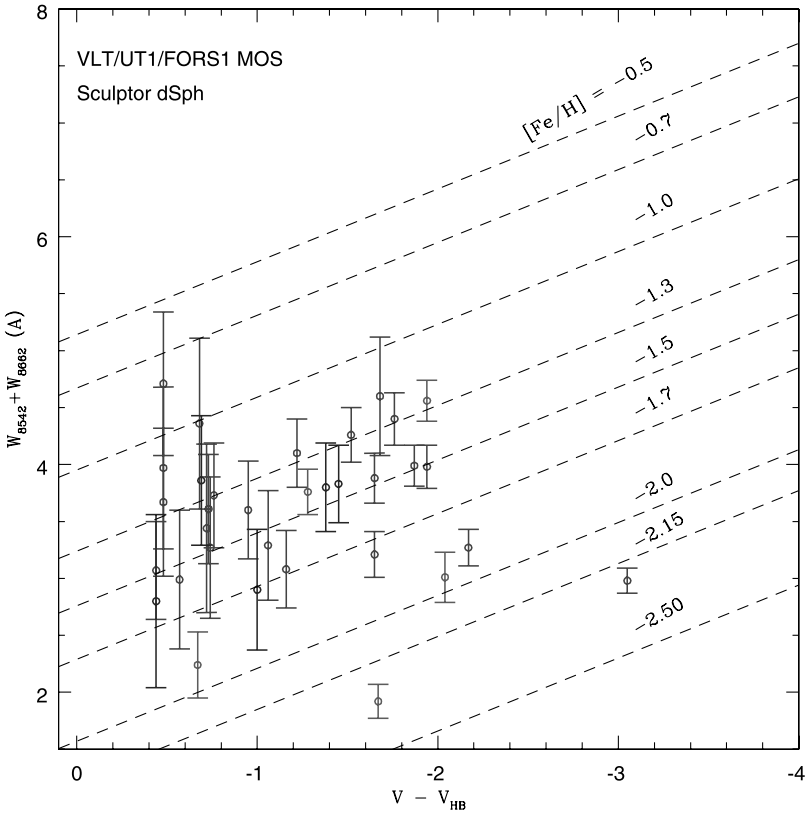

Figure 12. The summed equivalent width of the two stronger Ca II triplet lines is plotted against the *V* magnitude difference with the horizontal branch for the observed stars in the Sculptor dSph. Also plotted are lines of constant metallicity, as calibrated and checked with R97 in Fig. 10 (see Sections 3.2 and 4.1). The error bars come from the Gaussian fitting measurement errors.

(Thackeray 1950), clearly indicating that its stellar population contains a globular cluster age component. Various studies of evolved stars have shown Sculptor to contain a small number (eight) of intermediate-age carbon stars (e.g. Frogel et al. 1982; Azzopardi, Lequeux & Westerlund 1986), well-known indicators of metal-poor intermediate-age stellar populations (e.g. Aaronson et al. 1984) and possibly also anomalous Cepheids (Norris & Bessel 1978). The presence of old and intermediate age stellar populations clearly demonstrates that Sculptor is predominantly old, but there are signs that it has been forming some stars until at least 7–8 Gyr ago. Carignan et al. (1998) found evidence for small amounts of H I gas in and around Sculptor.

The first attempt to piece together an accurate star formation history determined from a CMD reaching down to globular cluster age main-sequence turn-offs was made by Da Costa (1984). He determined that the bulk of the stellar population of Sculptor is likely to be 2–3 Gyr younger than a typical globular cluster, such as M92. He also noted that the intrinsic width of the RGB was probably caused by a 0.5-dex, spread in abundance (from [Fe/H] = −2.1 to −1.6), and a population of 'blue stragglers' (in globular cluster terminology), which could be interpreted as main-sequence turn-off stars as young as 5 Gyr old, or they could be the results of stellar mergers. Kaluzny et al. (1995) made a careful study of the central region of Sculptor and found no main-sequence stars ($m_V < 21$), ruling out any star formation over the last 2 Gyr.

Using Wide Field Planetary Camera 2 (WFPC2) on the *Hubble Space Telescope* (*HST*), Monkiewicz et al. (1999) have made the deepest CMD of Sculptor to date; although they cover a tiny fraction of the entire galaxy, they detected stars several magnitudes below the oldest possible main-sequence turn-offs. Their accurate photometry in this region allowed them to conclude that the mean age of Sculptor is similar to that of a globular cluster, but that there was probably a spread in age during this epoch of at least 4 Gyr.

4.2.2 *Ca II triplet results*

In Table 5 we summarize the results for the sample of stars that we observed in Sculptor in the three fields across the galaxy, distributed as shown in Fig. 1. The nomenclature for the stars in Table 5 is that stars with c1 or c2 before a number are taken from the central field [a distinction is made between the two susi2 chips, i.e. c1 (east) and c2 (west)]. The north-eastern field is o1 and the south-western one is o2. The two outer fields were chosen to overlap with the Carignan et al. (1998) detections of H I. The positions of the selected stars in a CMD are shown in Fig. 4.

The Ca II triplet results are shown in a plot of equivalent width versus *V* magnitude difference from the horizontal branch, calibrated to the R97b results, in Fig. 12. Only stars that are considered to be members of Sculptor from their radial velocity, and to lie on the RGB, are fully included in Fig. 4. We have also excluded a number of stars because of their positions in the CMD. One star has a spectrum that looks like an M star, one lies in the horizontal branch region of the CMD, and four are too far to the blue side of the RGB, and are unlikely to be RGB stars. Since the Ca II triplet has only been shown to be valid for RGB stars, it is sensible to exclude these stars from our analysis. They are also plotted as crosses in Fig. 12.

It is clear that the red giants across Sculptor contain a significant spread in metallicity (see Fig. 13). The highest metallicity appears to be around [Fe/H] = −1.3, and there are a few objects

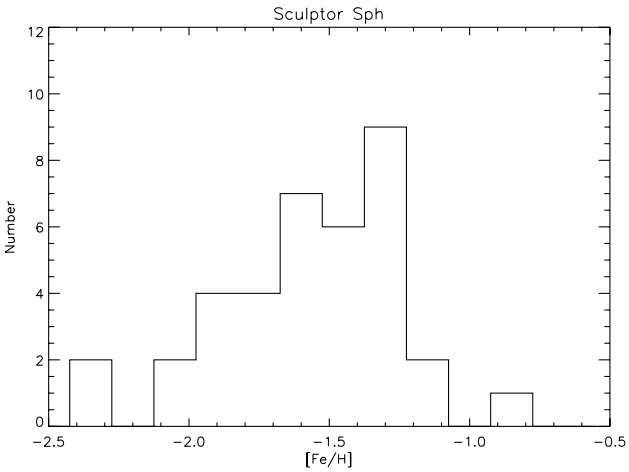

Figure 13. Here we plot the histogram distribution of Sculptor RGB Ca II triplet metallicities.

around [Fe/H] $= -2.1$, but the majority are clustered between [Fe/H] $= -2.0$ and -1.3. The mean metallicity of the stars that we observed in Sculptor is [Fe/H] $= -1.5 \pm 0.3$. There is no evidence for any spatial effect in the distribution of stars of different metallicity, and each of the observed fields (c1, c2, o1 and o2) contain stars that fall over the entire range of metallicity found for Sculptor. The histogram plot shows a fairly sharp cut-off in the upper metallicity boundary for Sculptor, with a shallow tail extending to low metallicity.

In general terms the Ca II triplet results give us a larger metallicity spread than we would expect from the breadth of the RGB observed in CMDs, as would be expected if the metal-poor stars were older than the metal-rich stars. Most of the stars seem to cluster around [Fe/H] ~ -1.5, which is slightly more metal-rich than the RGB suggested. This serves as a useful example of the inherent uncertainties caused by the age–metallicity degeneracy in determining metallicities from the RGB.

Another important point of note is that our results show that the colour of an individual star in Sculptor on the RGB is not a very good indicator of metallicity, not even of relative metallicity, across the RGB. There are blue stars from the metal-rich side of the metallicity distribution and red stars from the metal-poor side. There is, however, a slight general trend in the population of stars of different metallicity to be more red with higher metallicities, but there is a lot of dispersion. This also means that we often find that isochrones of the metallicity of the star we observe do not fit the $V - I$ colour of the star for any age. This reconfirms the fairly well-known fact that we do not understand stellar evolution on the RGB very well.

4.2.3 An evolutionary scenario

One possible global star formation history scenario for Sculptor, which takes into account all the information that we now have on the stellar population, is that Sculptor has undergone two distinct, possibly contiguous, phases of star formation during its lifetime.

The initial phase was probably the most intense. If the original gas was pristine then the enrichment was extremely rapid, because the mean metallicity of the stars from this epoch seems to be [Fe/H] ~ -1.7. The duration of this phase of active star formation was from 15 to11 Gyr ago, effectively an extended period of star formation beginning around the age of Galactic globular cluster formation, and continuing for about 4 Gyr. This assumption comes

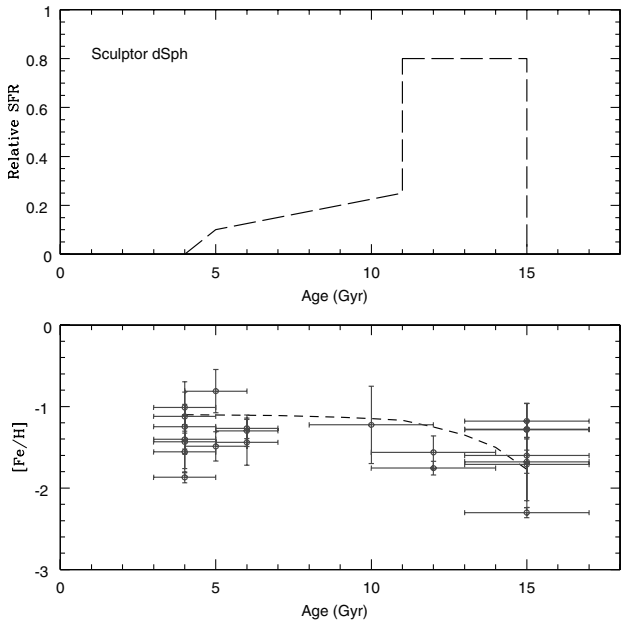

Figure 14. Here we display a possible star formation and chemical evolution scenario for Sculptor over its entire history (∼15 Gyr). In the upper panel is a schematic plot, consistent with all that we know of the stellar population of Sculptor, of how the rate of star formation may have varied over time, back from the epoch of globular cluster formation around 15 Gyr ago. In the lower panel we plot a corresponding variation in metallicity over the same time-frame. Over-plotted in the lower panel are our Ca II triplet measurements for individual RGB stars, for which we determined ages using isochrones.

from the deep CMD analysis of main-sequence turn-offs by Monkiewicz et al. (1999), and also from the theory of the horizontal branch morphology being caused by an age spread at early time (e.g. Da Costa 1984; Majewski et al. 1999).

The second phase of star formation in Sculptor is required to explain the population of intermediate-age evolved stars such as carbon stars, asymptotic giant branch stars and anomalous Cepheids. The average metallicity of these stars is [Fe/H] ~ -1.5. It is hard to give a higher age limit to these stars, but theory dictates that they are typically younger than 9 Gyr, and the limits on the brightest main-sequence objects makes the lower age limit for star formation 4–5 Gyr ago.

Whether these two phases are actually part of a continuous, though declining, star formation rate between 15 and 5 Gyr ago, or representative of two distinct epochs or perhaps 'bursts', it is hard to say for sure. It is only clear that star formation less than about 11 Gyr ago has to be much less intense than in the period between 11 and 15 Gyr ago because of the sparsely populated main-sequence at these ages, and relatively few intermediate-age stars.

Putting together all the pieces of information that we have about past star formation in Sculptor, one possible star formation history is plotted in the upper panel of Fig. 14 as a dashed line. The dashed line in the lower panel describes the most simple chemical evolution model (as first described by Searle & Sargent 1972), assuming the star formation history in the upper panel. We derived the assumed yield (the rate at which stars are producing Fe) by taking as fixed the high-metallicity end-point of the star formation history at the most recent time. On the lower plot we then over-plot where the RGB stars would lie, if we determined ages for the stars for which we measured the metallicity using isochrones (Bertelli et al. 1994). Our results are consistent with a trend of increasing

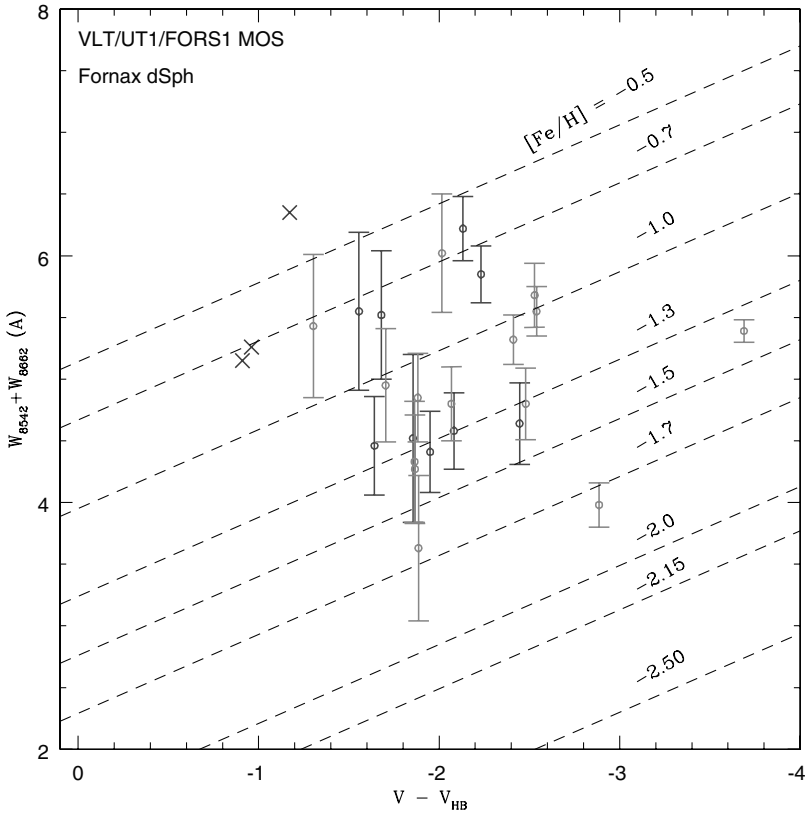

Figure 15. The summed equivalent width of the two stronger Ca II triplet lines is plotted, as described in Fig. 12.

metallicity with time since formation, but there is a large scatter at all ages. There appears to a broad agreement between the trends seen in the data points and in the model.

4.3 Fornax dwarf spheroidal

4.3.1 Background

The discovery of Fornax was presented in the same paper as the discovery of Sculptor (Shapley 1938), and they make an interesting pair for comparison. Qualitatively they look very similar, although Fornax is larger and more metal-rich in the mean, and has globular clusters, whereas Sculptor has none. Also, looking in detail at the star formation histories of Sculptor and Fornax, it is clear that they have followed very different evolutionary paths. Sculptor is dominated by older stellar populations, whereas Fornax appears to have been forming stars quite actively until 2 Gyr ago, and to be dominated by a 4–7 Gyr old population, and has evidence for only a small number of globular cluster age stars in its field population.

Fornax contains a large number of RR Lyrae and Mira variables and carbon stars, as well as one anomalous Cepheid, one planetary nebula and five globular clusters (Da Costa 1998). Young (1999) looked for neutral hydrogen, and found none. The best estimate for the mean abundance of the bulk of the stars in Fornax comes from the intrinsic width of the RGB, and is [Fe/H] $= -1.4$ with a spread of about 0.15 dex (Buonanno et al. 1985). It is quite hard to disentangle age from metallicity effects on the RGB because Fornax has such a long-lasting and complex star formation history.

The extended sequence of main-sequence turn-offs in the Fornax CMD indicates a long history of star formation (e.g. Beauchamp et al. 1995; Stetson, Hesser & Smecker-Hane 1998; Buonanno et al. 1999), which has only recently ceased. The luminosity of the brightest blue stars shows that Fornax cannot contain any stars younger than 100 Myr (Stetson et al. 1998).

The presence of numerous ($\sim$120) carbon stars with a wide range of bolometric luminosities indicates a significant mass dispersion among the progenitors, and hence a significant age spread in the range 2–8 Gyr ago (e.g. Aaronson & Mould 1980, 1985; Azzopardi et al. 1999). This is supported by a well-populated intermediate-age subgiant branch and a red clump, which require a significant population with an age of 2–4 Gyr. Most recently, a *HST* study sampling the main-sequence turn-offs of the intermediate-age and old populations in the centre of Fornax was carried out by Buonanno et al. (1999), and they found evidence for a highly variable star formation history starting at the epoch of globular cluster formation (say 15 Gyr ago) and continuing until 0.5 Gyr ago. Their detailed analysis did not take account of metallicity variations with age, which must be present, and which will probably make their ages roughly 30 per cent too young, in the mean.

An old population is present as demonstrated by detection of a red horizontal branch, slightly fainter than the red clump (Buonanno et al. 1999), and of RR Lyrae variables (Stetson et al. 1998). In addition to the large number of RR Lyrae variables, there is also a weak, blue horizontal branch, so Fornax clearly does contain a very old, metal-poor component.

4.3.2 Ca II triplet results

In Table 6 we summarize the results for the sample of stars that we observed in Fornax in a field in the centre of the galaxy, positioned as shown in Fig. 2. Where the observed stars lie in a CMD is shown in Fig. 5. The Ca II triplet results are presented on a plot of

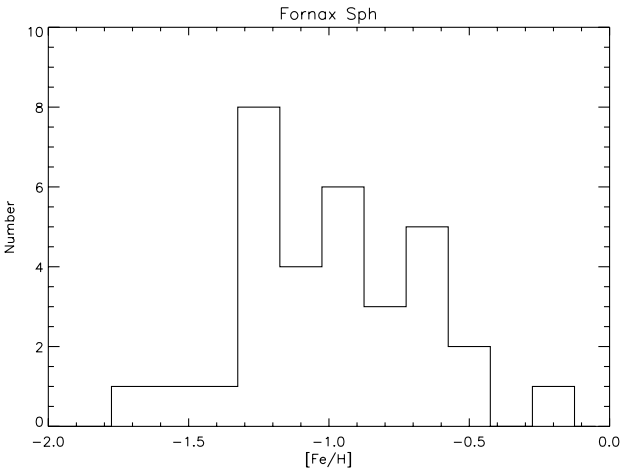

Figure 16. Here we plot the histogram distribution of Fornax RGB Ca II triplet metallicities.

equivalent width versus V magnitude difference from the horizontal branch, calibrated to the R97b results, in Fig. 15. Only stars that are considered to be members of Fornax from their radial velocity, and which lie on the RGB, are fully included in Fig. 15; we have plotted the location (with crosses) where the stars of low signal-to-noise ratio lie, without their corresponding error bars (see Table 6). This is done in the interests of not making Fig. 15 unduly confusing. Fig. 15 suggests that the bulk of stars in Fornax lie between [Fe/H] $= -1.5$ and -0.7, with a mean value of -1.0 ± 0.3. The total metallicity spread that we find for Fornax is 0.6 dex, and it is more skewed towards higher metallicities than is consistent with that expected from the width of the RGB. There are apparently a few outliers at lower metallicity, [Fe/H] ~ -1.5, and at higher metallicity, [Fe/H] ~ -0.5. The abundance distribution is plotted as a histogram in Fig. 16. In contrast to Sculptor, Fornax has more of a sharp cut-off in the metallicity distribution at low metallicities, with a tail of values going out to higher metallicity values. The peak of the distribution is at about [Fe/H] $= -1.2$.

As with Sculptor, the red giants selected across Fornax contain a significant spread in metallicity, but not surprisingly our results and previous photometric determinations of both the mean and the spread in metallicity do not agree. The metallicities that we measure are higher and the spread is greater than the photometric determinations. This is because Fornax contains a very large spread in age and is dominated by intermediate-age stars, and so using globular cluster RGB fiducials is going to lead to incorrect results, as the majority of Fornax stars are considerably younger than globular cluster stars. This is why we find that the mean metallicity of Fornax is higher than previously thought. We do not have much information on the spatial variation of metallicity in Fornax, as both our (relatively small) spectroscopic fields of view lie in the central region of the galaxy, but over the region we do cover there is no evidence for spatial variation in metallicity.

As for Sculptor, there is no correlation between the colour of a star on the RGB and the metallicity that we measure from the Ca II triplet lines in Fornax. The more metal-rich and more metal-poor populations overlie each other very closely. Unlike Sculptor, however, the range of metallicities and colours does match with the colour range of the available isochrones at the metallicity of most of the stars. This suggests that as we go to higher metallicities, the stellar evolution models do a better job on the RGB.

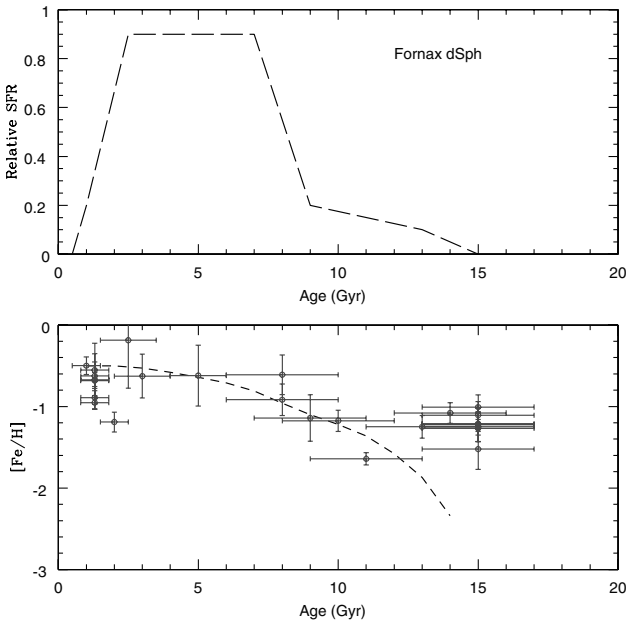

Figure 17. Here we display a possible star formation and chemical evolution scenario for Fornax over its entire history (∼15 Gyr), as described in Fig. 14.

4.3.3 An evolutionary scenario

One possible global star formation history scenario for Fornax which takes into account all the information that we now have on its stellar population could be that, unlike Sculptor, Fornax appears to have maintained some level of star formation more or less continuously over most of its history until for the last few hundred million years. It is also possible that the present gap in star formation is temporary, although it is then hard to understand where the gas for future generations is now. The main justification for this scenario comes from the *HST* CMD analysis of (admittedly) a small fraction of the stellar population of Fornax (Buonanno et al. 1999), and also the apparently uniform distribution of Ca II triplet metallicities seen in our sample of RGB stars.

There is clear evidence in the evolved field stars of Fornax for very old stars from a blue horizontal branch and RR Lyrae stars, and also an extensive intermediate-age stellar population with an He-burning red clump and carbon stars. None of these indicators can be accurately transformed into a star formation rate at any of these times, except perhaps that the unusually high fraction of carbon stars in Fornax suggests that a large fraction of the stellar population of Fornax was formed roughly between 1 and 9 Gyr ago, and the red clump suggests a high star formation rate between 2 and 4 Gyr ago. These deductions can be refined and confirmed by the *HST* CMD main-sequence turn-offs, which suggest a dominant peak in star formation activity between 2.5 and 9 Gyr ago, with relatively very little star formation in the last 2.5 Gyr. It is complicated to quantify what may have happened more than 9 Gyr ago. It seems from the main-sequence turn-off information that more than 9 Gyr ago the star formation rate was much lower than during the peak period, 2.5–9 Gyr ago. There is, however, the matter of the five globular clusters to consider. Common wisdom says that globular clusters accompany episodes of intense star formation in the host galaxies (e.g. Baade 1963). This is, however, ambiguous from the perspective of the dwarf galaxies of the Local Group (e.g. van den Bergh 2000), including Fornax.

Putting together all the pieces of information we have about past star formation in Fornax (but ignoring the presence of globular clusters), one possible star formation history is plotted in the upper panel of Fig. 17. Using this star formation history we estimate what the accompanying metallicity evolution might have been, and this is plotted as a dashed line in the lower panel of Fig. 17. We have assumed a simple chemical evolution model (as first described by Searle & Sargent 1972). We have derived the assumed yield (the rate at which stars are producing Fe) by taking as fixed the high-metallicity end-point of the star formation history at the most recent time. Also plotted on this lower diagram are where the RGB stars that we observed would lie if we determined ages using isochrones (Bertelli et al. 1994). The trend for metallicity with age is clearly increasing with time towards the present, but there is quite a lot of scatter, especially for those stars that appear to be very young. This might be due to problems in matching the low-metallicity stellar evolution tracks to our observations, which was also found to be a problem in Sculptor. As the metallicity of the stellar population gets lower, the difference in $V-I$ colour of a 15-Gyr-old star versus a 2-Gyr-old star on the RGB in the theoretical models dramatically declines. At [Fe/H] $= -0.7$ the difference is about 0.14 mag, but at [Fe/H] $= -1.9$ it is about 0.04 mag. Therefore tiny reddening or photometric offsets for low-metallicity stars will have a dramatic impact on the perceived age of an RGB star. There appears to be an offset in the basic metallicity trend between the simple model and the data points at ages >12 Gyr. This is the most uncertain region in which to interpret the star formation history from the CMD, but as it stands it might suggest that there has been some kind of initial enrichment of the gas in Fornax at very early times. This could perhaps be a relic of the epoch of globular cluster formation which appears to pre-date that of the majority of star formation in the field population of Fornax.

4.4 NGC 6822

4.4.1 Background

NGC 6822 is one of our closest neighbouring dwarf irregular type galaxies. It was nominally discovered by Barnard (1884), although it was not understood as neighbouring galaxy until Hubble (1925) discovered Cepheid variable stars and determined it as being much more distant than even the furthest globular clusters, and thus truly extragalactic. It is quite similar to the Small Magellanic Cloud, but it is smaller and less luminous, and unlike the Small Magellanic Cloud it is not involved in any (obvious) interaction with our Galaxy or any other galaxy. Unfortunately NGC 6822 is at very low Galactic latitude, and therefore suffers from large and varied reddening over the whole galaxy, and there is also a considerable problem of foreground stellar contamination when accurately determining its stellar content. Despite these issues, its proximity makes it a very rewarding object in which to study the properties of young (relatively) low-metallicity stars in an isolated star-forming dwarf irregular galaxy.

Unlike Sculptor or Fornax, NGC 6822 is presently actively forming stars. It contains numerous H II regions, some extremely luminous, spread over the face of the galaxy (e.g. Hodge, Lee & Kennicutt 1988; O'Dell, Hodge & Kennicutt 1999), and various studies have catalogued the massive star content (e.g. Westerlund et al. 1983; Armandroff & Massey 1985). NGC 6822 has a large extended halo of H I gas (Brandenburg & Skillman 1998; de Blok & Walter 2000), going out well beyond the optical galaxy. There have been detailed abundance studies of young A-type supergiants (Muschielok et al. 1999; Venn et al. 2001), and all the young stars looked at to date reveal an iron abundance of [Fe/H] ~ -0.50, confirming that NGC 6822 has a slightly higher present-day abundance than the Small Magellanic Clouds, consistent with H II region metallicities (e.g. Pagel, Edmunds & Smith 1980). NGC 6822 also contains a number of star cluster candidates (Wyder et al. 2000), although only one remains as a likely 'true' ancient globular cluster candidate, similar to those found around our Galaxy. Even one ancient globular cluster is quite unusual for dwarf irregular galaxies in the Local Group.

Cook, Aaronson & Norris (1986) detected a significant population of intermediate-age carbon stars with a wide luminosity variation (suggesting a large age range), and a significant extended asymptotic giant branch population was detected by Gallart et al. (1994). The clear presence of large numbers of these evolved stars shows that NGC 6822 must have had quite a high star formation rate during some or all of the period 1–9 Gyr ago. There has been an extensive series of papers modelling the entire star formation history of NGC 6822 from the resolved stars in a CMD by Gallart et al. (1996a,b,c). Although this work is extremely detailed and represents a noble attempt to dig out information from a noisy CMD, their analysis is based on data taken with a 2.5-m telescope, and so the magnitude limits are such that the main-sequence turn-offs cannot be detected for stars older than about 400 Myr, and so their results on star formation before this time come solely from the evolved red stellar population of the upper RGB. This is subject to a great deal of uncertainty, especially without any independent metallicity information. There is little or nothing known about the stellar population older than about 9 Gyr in NGC 6822. The only CMD that reaches to the horizontal branch luminosity comes from the analysis of field star contamination in *HST* studies of NGC 6822 star clusters, and has not yet been carefully analysed in terms of a star formation history. The main sequence in the *HST* CMDs does not show any obvious evidence for strong or sharp variations in the star formation rate with time over the past Gyr. There is also only evidence for a very weak horizontal branch in these data. For the purposes of using the AD91 correction for the effects of luminosity to the Ca II triplet results, we estimated $V_{\rm HB}$ from Wyder et al. to be 24.6. A search for RR Lyrae stars did not show them to be present in any significant numbers (Saha, private communication), and this study was contemporaneous with other searches by the same investigators, who successfully discovered RR Lyrae stars in several other galaxies, including IC 1613 (Saha et al. 1992). This supports the *HST* results, which covered only a small field of view, that the horizontal branch, if present, is weak in NGC 6822. This galaxy is clearly dominated by intermediate-age and perhaps even young stellar populations.

The distance modulus of NGC 6822 is nearly 3 mag more distant than Fornax, and 4 mag more distant than Sculptor. Thus these observations of individual RGB stars are really pushing the capabilities of FORS1 on UT1.

4.4.2 Ca II triplet results

In Table 7 we summarize the results for the sample of stars that we observed in NGC 6822 in the NTT field observed at the position north of the centre of the galaxy, shown in Fig. 3. The nomenclature for the stars in Table 7 is that stars with the prefix s1 are from the eastern half of the NTT field, and those with the prefix s2 are from the western half of the field. Those stars with prefix s1b refer to a second series of observations on the eastern

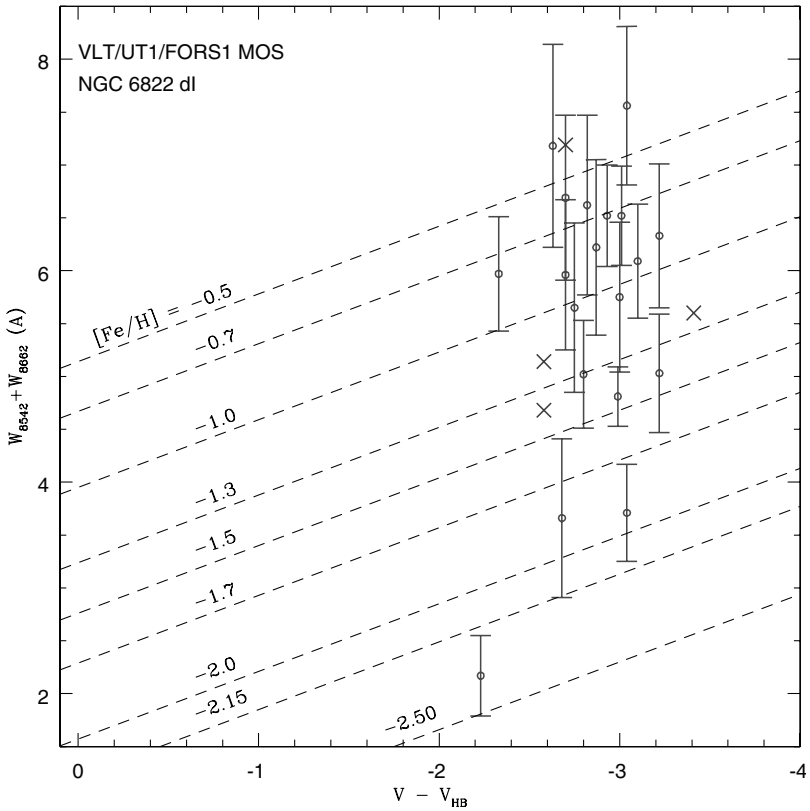

Figure 18. The summed equivalent width of the two stronger Ca II triplet lines is plotted, as described in Fig. 12.

field, but for some reason they were of much poorer signal-to-noise ratio than the s1 data.

The Ca II triplet results are shown on a plot of equivalent width versus V magnitude difference from the horizontal branch (see Table 1), calibrated to the R97b results, in Fig. 18. Only stars that are considered to be members of NGC 6822 from their radial velocity, and which lie on the RGB, are included in Fig. 18; we have plotted the location (with crosses) of where the particularly low signal-to-noise ratio stars lie, but without their error bars (see Table 7). Note that there is a larger than usual uncertainty in the horizontal branch magnitude, and there is almost certainly variable reddening across NGC 6822. We have assumed a constant reddening $[E(B-V) = 0.26]$ for all stars observed; if there is indeed a large scatter about this value, this will artificially create a scatter in metallicity, but this will almost certainly remain much less than the intrinsic equivalent width measurement errors.

Although the error bars are large, it appears that the red giants across the NGC 6822 field that we observed contain a significant spread in metallicity, which is larger than that seen in either Sculptor or Fornax. The highest metallicity appears to be around [Fe/H] $= -0.5$, and there are a few objects that fall around [Fe/H] $= -2$. The mean metallicity of the stars that we observe is [Fe/H] $= -1 \pm 0.5$. We do not see any evidence for spatial variations, but we are observing a rather small area of NGC 6822. Our upper (young) metallicity measurements are consistent with existing accurate young star and H II region abundances for this galaxy, which consistently find [Fe/H] $= -0.5$. NGC 6822 thus appears to contain stars across the entire metallicity range to which we are sensitive ([Fe/H] > -2.5), unlike Fornax, which appears to contain only stars more metal-rich than [Fe/H] > -1.7, or Sculptor which contains only stars more metal-poor than [Fe/H] < -1.3. The distribution of metallicities as a histogram (Fig. 19) also looks different from either Sculptor or Fornax. It has a central peak at [Fe/H] $= -0.9$ with a roughly equal distribution of stars to the metal-rich and metal-poor sides of this peak.

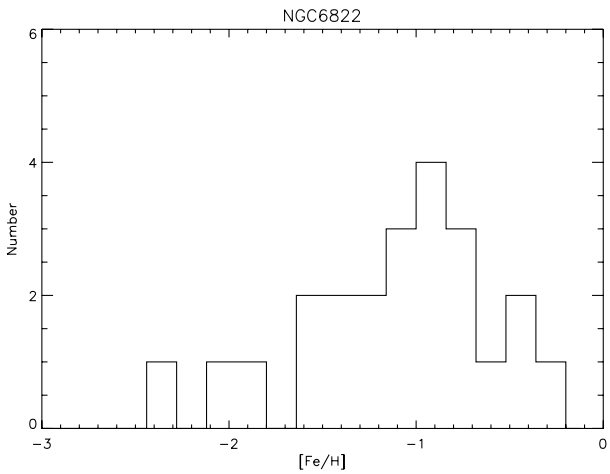

Figure 19. Here we plot the histogram distribution of NGC 6822 RGB Ca II triplet metallicities.

4.4.3 An evolutionary scenario

The most striking aspect of Figs 18 and 19 is the large range in metallicity, but, because of the problems with variable reddening and because the star formation history of NGC 6822 is not constrained in detail beyond about 400 Myr ago, it is more difficult

to fit the Ca II triplet observations accurately into a detailed picture of the star formation history of NGC 6822. Thus our attempt is much more speculative than for Sculptor or Fornax. Our uncertain knowledge about the detailed star formation history is compounded by a combination of poorer signal-to-noise ratio spectra and variable and uncertain reddening towards NGC 6822.

Putting together what information we have results in a plausible star formation history in the upper panel of Fig. 20. This is derived from the results of Gallart et al. (1996a), the carbon star survey of Cook et al. (1986), and the interpretation of the extended asymptotic giant branch of Gallart et al. (1994) as being indicative of a fairly recent (∼3 Gyr ago) burst of star formation (see Lynds et al. 1998). In the lower panel we plot, as a dashed line, what might be a corresponding metallicity evolution, assuming the star formation history given in the upper panel. We have assumed a simple chemical evolution model (as first described by Searle & Sargent 1972). We have derived the assumed yield (the rate at which stars are producing Fe) by taking as fixed the high-metallicity end-point of the star formation history at the most recent time. Also plotted in this lower diagram are the RGB stars that we observed, if we use isochrones (Bertelli et al. 1994) to determine their ages. There were a large number of stars in NGC 6822 that were significantly too red to match any isochrone at their metallicity, presumably because of increased reddening, and these stars were not included in Fig. 20. Also plotted in the lower panel of Fig. 20 is the Venn et al. (2001) direct measurement of the iron abundance of two (young) supergiant stars in NGC 6822; this is the present-day metallicity of the galaxy. In Fig. 20 the significant rise in the star formation rate of NGC 6822 which occurred at some point in the last 2–3 Gyr is consistent with a relatively recent surge in the metallicity of NGC 6822, as exhibited by the metallicity spread of the RGB stars in this age range. There are also a number of old, metal-poor RGB stars, which appear to come from a period before this recent increase in star formation activity. Since the low

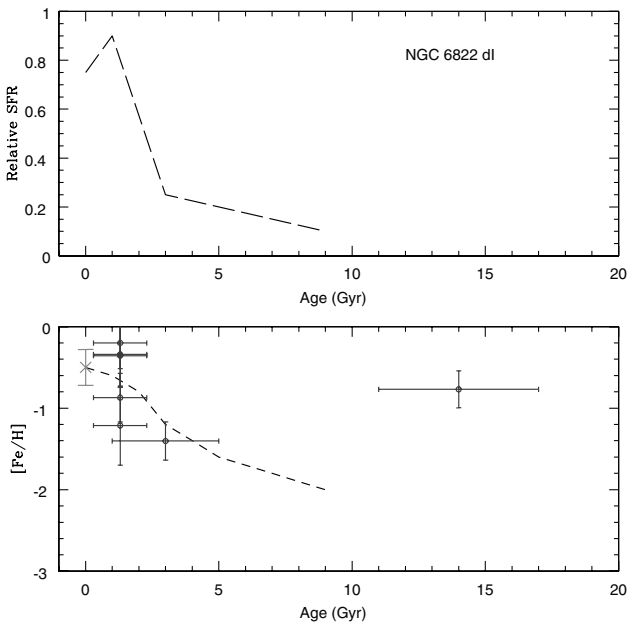

Figure 20. Here we display a highly speculative possible star formation and chemical evolution scenario for NGC 6822 over its entire history (∼15 Gyr), as described in Fig. 14. There is an additional point for the present-day metallicity measured from B supergiant spectra by Venn et al. (2001).

end of the Ca II triplet metallicity is around [Fe/H] = −2.4, and there is little evidence for a large old population, with only a very weak horizontal branch population, there is unlikely to have been very much star formation during ancient times in this galaxy. It is hard to make a firm conclusion as to how good a match the data points are to a simple chemical evolution model. Our results are broadly consistent with a trend of increasing metallicity with time since formation over the last few Gyr. The single point at 14 Gyr, however, if we chose to believe it, does suggest that the metallicity evolution of this system has not been straightforward, although detailed analysis of possible scenarios is premature with these sparse data. We await more sensitive observations in the future.

5 CONCLUSIONS

We have presented spectroscopic metallicity distribution functions for RGB stars in three nearby galaxies, which are more precise than photometric estimates, and it is the first time that old-star metallicity estimates have been made for NGC 6822. We have attempted to reconcile photometric determinations of star formation histories from CMD analysis and spectroscopic abundance determinations from Ca II triplet equivalent widths into a single star formation and chemical evolution scenario over the period 1–15 Gyr ago for three nearby galaxies.

All three galaxies that we have studied have clearly had very different evolutionary paths, in star formation history and thus not surprisingly in metallicity evolution as well. The CMD analysis and the Ca II triplet results give broadly consistent results, but there are some discrepancies which mean that studies like this are worthwhile. The Ca II triplet results allow us additional insight in to modelling the evolution of a galaxy in terms of the two most fundamental parameters – star formation rates and chemical evolution – and we are thus measuring these parameters independently through time, and thus accurately determining the population box of each galaxy (cf. Hodge 1989).

The mean metallicity of the RGB stars that we observed in our sample of galaxies increases with the mass of the galaxy, as would be predicted by theory (e.g. Ferrara & Tolstoy 2000). Thus Sculptor is the least massive of the three galaxies (6×10^6 $M_\odot$) and it also has the lowest mean metallicity, [Fe/H] = −1.6. Fornax is about 10 times more massive (7×10^7 $M_\odot$), and it has a mean metallicity about three times greater, [Fe/H] = −1.1. NGC 6822 is roughly another order of magnitude more massive (2×10^9 $M_\odot$), and the metallicity of the RGB stars that we observed has a very large spread, but the mean [Fe/H] = −0.9, so is a factor of about 1.5 greater than Fornax. The distribution of the metallicities of the stars in each of the galaxies is very different, as can be seen by comparing Figs 13, 16 and 19. Although we are observing a small sample of the RGB stars in each galaxy, they were randomly selected across the width of the RGB, and so we can conclude that the different distribution of metallicity means that each galaxy has had a different enrichment history, consistent with their different star formation histories.

Sculptor is a galaxy where the star formation history was apparently truncated about 4–5 Gyr ago, Fornax is a galaxy which had a fairly continuous star formation rate over most of its history until a few hundred million years ago, and NGC 6822 has apparently enjoyed at least one relatively recent enhancement in its star formation rate. Thus all of these galaxies have experienced varying star formation rates over extended time-periods.

One might speculate that Sculptor was formed from nearly pristine gas, which was rapidly enriched in an ancient episode of

star formation which also formed a large fraction of the stars in the galaxy. Star formation then continued at a lower rate until it was sharply cut off about 4–5 Gyr ago, when the metallicity of the stars being formed was [Fe/H] = −1.2. This would explain the sharp high-metallicity cut-off in Fig.13. Fornax, on the other hand, looks more like a galaxy that formed most of its stars out of pre-enriched gas, perhaps starting around 10 Gyr ago, at [Fe/H] = −1.3. This explains the sharp low-metallicity cut-off in Fig. 16. It is possible that the gas out of which the stars in the Fornax galaxy were formed was pre-enriched by the formation of its globular cluster population about 15 Gyr ago, and most of the star formation in the galaxy did not begin until several Gyr after this time. The metallicity distribution of NGC 6822 looks like a combination of both Sculptor and Fornax, suggesting that it formed stars from very early times, but at a low rate, which increased up to a maximum quite recently, and is now decreasing again. Probably if gas were removed from NGC 6822 about 4–5 Gyr ago it would look similar in most respects to a metal-rich Sculptor rather than Fornax, and we can thus speculate that the main difference between Sculptor and NGC 6822 is that NGC 6822 was massive enough to keep its gas up to the present day (see Ferrara & Tolstoy 2000). NGC 6822 is clearly a galaxy which should be more carefully studied in the future.

ACKNOWLEDGMENTS

We thank Evan Skillman, Andrea Ferrara and Kim Venn for useful discussions, and the Paranal Observatory Science Operations staff, especially Thomas Szeifert, Andreas Kaufer and Chris Lidmam for the excellent support that we received during this run. This paper is based on observations collected at the European Southern Observatory, proposal numbers 63.N-0603 and 61.A-0275. IRAF is distributed by the National Optical Astronomy Observatories, which are operated by the Association of Universities for Research in Astronomy, Inc., under cooperative agreement with the National Science Foundation. Also based on photographic data obtained using the UK Schmidt Telescope. The UK Schmidt Telescope was operated by the Royal Observatory Edinburgh, with funding from the UK Science and Engineering Research Council, until 1998 June, and thereafter by the Anglo-Australian Observatory. Original plate material is copyright © the Royal Observatory Edinburgh and the Anglo-Australian Observatory. The plates were processed into the present compressed digital form with their permission. The Digitized Sky Survey was produced at the Space Telescope Science Institute under US Government grant NAG W-2166.

REFERENCES

Aaronson M., Mould J. R., 1980, ApJ, 240, 804
Aaronson M., Mould J. R., 1985, ApJ, 290, 191
Aaronson M., Da Costa G. S., Hartigan P., Mould J. R., Norris J., Stockman H. S., 1984, ApJ, 277, 9
Armandroff T. E., Da Costa G. S., 1986, AJ, 92, 777
Armandroff T. E., Da Costa G. S., 1991, AJ, 101, 1329 (AD91)
Armandroff T. E., Massey P., 1985, ApJ, 291, 685
Armandroff T. E., Zinn R., 1988, AJ, 96, 92
Azzopardi M., Lequeux J., Westerlund B. E., 1986, A&A, 161, 232
Azzopardi M., Breysacher J., Muratorio G., Westerlund B. E., 1999, in Whitelock P., Cannon R., eds, Proc. IAU Symp. 192, The Stellar Content of Local Group Galaxies. Astron. Soc. Pac., San Francisco, p. 9
Baade W., 1963, in Payne-Gaposchkin C., ed., Evolution of Stars and Galaxies. Harvard Univ. Press, Cambridge MA
Baade W., Hubble E., 1939, PASP, 51, 40
Barnard E. E., 1884, The Sidereal Messenger, 3, 254
Beauchamp D., Hardy E., Suntzeff N. B., Zinn R., 1995, AJ, 109, 1628
Bertelli G., Bressan A., Chiosi C., Fagotto F., Nasi E., 1994, A&AS, 106, 275
Brandenburg H. J., Skillman E. D., 1998, BAAS, 193, 701
Brown J. A., Wallestein G., 1993, AJ, 106, 133
Brown J. A., Wallestein G., Zucker D., 1997, AJ, 114, 180
Buonanno R., Buscema G., Corsi C. E., Iannicola G., Fusi Pecci F., 1983, A&AS, 51, 83
Buonanno R., Corsi C. E., Fusi Pecci F., Hardy E., Zinn R., 1985, A&A, 152, 65
Buonanno R., Buscema G., Fusi Pecci F., Richer H. B., Fahlmann G. G., 1990, AJ, 100, 1811
Buonanno R., Corsi C. E., Castellani M., Marconi G., Fusi Pecci F., Zinn R., 1999, AJ, 118, 1671
Carignan C., Beaulieu S., Côté S., Demers S., Mateo M., 1998, AJ, 116, 1690
Carney B. W., 1996, PASP, 108, 900
Carretta E., Gratton R. G., 1997, A&AS, 121, 95
Cole A. A., 1998, ApJ, 500, L137
Cole A. A. et al., 1999, AJ, 118, 1657
Cole A. A., Smecker-Hane T. A., Gallagher J. S., 2000, AJ, 120, 1808
Cook K. H., Aaronson M., Norris J., 1986, ApJ, 305, 634
Da Costa G. S., 1984, ApJ, 285, 483
Da Costa G. S., 1998, in Aparicio A., Herrero A., Sanchez F., eds, Stellar Astrophysics for the Local Group. Cambridge Univ. Press, Cambridge, p. 351
Da Costa G. S., Armandroff T. E., 1986, AJ, 92, 777
Da Costa G. S., Armandroff T. E., 1990, AJ, 100, 162
Da Costa G. S., Hatzidimitriou D., 1998, AJ, 115, 1934
Da Costa G. S., Armandroff T. E., Norris J. E., 1992, AJ, 104, 154
de Blok W. J. G., Walter F., 2000, ApJ, 537, L95
Edvardsson B., Andersen J., Gustafsson B., Lambert D. L., Nissen P. E., Tomkin J., 1993, A&A, 275, 101
Ferrara A., Tolstoy E., 2000, MNRAS, 313, 291
Frogel J. A., Blanco V. M., Cohen J. G., McCarthy M. F., 1982, ApJ, 252, 133
Gallart C., Aparicio A., Chiosi C., Bertelli G., Vílchez J. M., 1994, ApJ, 425, L9
Gallart C., Aparicio A., Vílchez J. M., 1996a, AJ, 112, 1928
Gallart C., Aparicio A., Bertelli G., Chiosi C., 1996b, AJ, 112, 1950
Gallart C., Aparicio A., Bertelli G., Chiosi C., 1996c, AJ, 112, 2596
Hargreaves J. C., Gilmore G., Irwin M. J., Carter D., 1994, MNRAS, 269, 957
Harris W. E., 1996, AJ, 112, 1487
Harris W. E., Canterna R., 1980, ApJ, 239, 815
Hodge P., 1989, ARA&A, 27, 139
Hodge P., Lee M. G., Kennicutt R. C., 1988, PASP, 100, 917
Hubble E., 1925, ApJ, 62, 409
Hughes J., Wallerstein G., 2000, AJ, 119, 1225
Kaluzny J., Kubiak M., Szymanski M., Udalski A., Krzeminski W., Mateo M., 1995, A&AS, 112, 407
Kunkel W. E., Demers S., 1977, ApJ, 214, 21
Lynds R., Tolstoy E., O'Neil E. J., Hunter D. A., 1998, AJ, 116, 146
Majewski S. R., Siegel M. H., Patterson R. J., Rood R. T., 1999, ApJ, 520, L33
Mateo M., 1998, ARA&A, 36, 435
Mateo M., Olszewski E., Welch D. L., Fischer P., Kunkel W., 1991, AJ, 102, 914
Matteucci F., Tosi M., 1985, MNRAS, 217, 391
Monkiewicz J. et al., 1999, PASP, 111, 1392
Muschielok B. et al., 1999, A&A, 325, L40
Norris J., Bessel M. S., 1978, ApJ, 225, L49
O'Dell C. R., Hodge P. W., Kennicutt R. C., 1999, PASP, 111, 1382
Olszewski E. W., Schommer R. A., Suntzeff N. B., Harris H. C., 1991, AJ, 101, 515
Osterbrock D. E., Martel A., 1992, PASP, 104, 76
Pagel B. E. J., Tautvaišienė G., 1998, MNRAS, 299, 535
Pagel B. E. J., Edmunds M. G., Smith G., 1980, MNRAS, 193, 219
Queloz D., Dubath P., Pasquini L., 1995, A&A, 300, 31

Richter O.-G., Tammann G. A., Huchtmeier W. K., 1987, A&A, 171, 33
Rutledge G. A., Hesser J. E., Stetson P. B., Mateo M., Simard L., Bolte M., Friel E. D., Copin Y., 1997a, PASP, 109, 883, (R97a)
Rutledge G. A., Hesser J. E., Stetson P. B., 1997b, PASP, 109, 907 (R97b)
Saha A., Freedman W. L., Hoessel J. G., Mossman A. E., 1992, AJ, 104, 1072
Searle L., Sargent W. L. W., 1972, ApJ, 173, 25
Searle L., Wilkinson A., Bagnuolo W. G., 1980, ApJ, 239, 803
Shapley H., 1938, Harvard Bull., 908, 1
Shetrone M. D., Côté P., Sargent W. L. W., 2001, ApJ, 548, 592
Smecker-Hane T. A., McWilliam A., 1999, in Hubeny I., Heap S., Cornett R. P., eds, ASP Conf. Ser. Vol. 192, Spectrophotometric Dating of Stars and Galaxies. Astron. Soc. Pac., San Francisco, p. 150
Sneden C., Kraft R. P., Shetrone M. D., Smith G. H., Langer G. E., Prosser C. F., 1997, AJ, 114, 1964
Stetson P. B., Hesser J. E., Smecker-Hane T. A., 1998, PASP, 110, 533
Suntzeff N. B., Mateo M., Terndrup D. M., Olszewski E. W., Geisler D., Weller W., 1993, ApJ, 418, 208
Thackeray A. D., 1950, Observatory, 70, 144
Tolstoy , 1998, in Whitelock P., Cannon R., eds, Proc. IAU Symp. 192, The Stellar Content of Local Group Galaxies. p. 218
Tolstoy E., Irwin M. J., 2000, MNRAS, 318, 1241
Tolstoy E., Gallagher J. S., Greggio L., Tosi M., De Marchi G., Romaniello M., Minniti D., Zijlstra A. A., 2000, ESO Messenger, 99, 16
van den Bergh S., 2000, PASP, 112, 932
Venn K. A. et al., 2001, ApJ, 547, 765
Westerlund B. E., Azzopardi M., Breysacher J., Lequeux J., 1983, A&A, 123, 159
Wyder T. K., Hodge P. W., Zucker D. B., 2000, PASP, 112, 1162
Young L. M., 1999, AJ, 117, 1758
Zinn R., West M. J., 1984, ApJS, 55, 45

APPENDIX A: TABLES GIVING POSITIONS OF THE OBSERVED STARS

Table A1. Sculptor positions.

Star	RA	Dec. (J2000)
c1-56	01:00:01.3	−33:45:16
c1-70	01:00:02.9	−33:44:59
c1-85	01:00:04.8	−33:44:41
c1-68	01:00:02.9	−33:44:06
c1-101	01:00:06.9	−33:43:45
c1-99	01:00:06.7	−33:43:05
c1-43	00:59:59.7	−33:42:37
c1-55	01:00:01.1	−33:42:22
c1-67	01:00:02.8	−33:42:00
c1-76	01:00:03.9	−33:41:40
c1-81	01:00:04.6	−33:41:13
c1-46	01:00:00.1	−33:40:57
c1-47	01:00:00.1	−33:40:41
c1-88	01:00:05.5	−33:40:17
c1-78	01:00:04.0	−33:40:02
c2-64	01:00:17.1	−33:45:13
c2-81	01:00:19.0	−33:44:52
c2-88	01:00:19.9	−33:44:24
c2-73	01:00:18.0	−33:44:12
c2-38	01:00:13.4	−33:43:38
c2-39	01:00:13.5	−33:43:20
c2-72	01:00:17.8	−33:43:04
c2-52	01:00:15.5	−33:42:37
c2-27	01:00:12.3	−33:42:08
c2-60	01:00:16.8	−33:41:46
c2-86	01:00:19.8	−33:41:12
c2-82	01:00:19.5	−33:40:36
c2-53	01:00:15.9	−33:40:15
c2-85	01:00:19.8	−33:40:04
o1-1	01:00:42.8	−33:31:30
o1-4	01:00:43.3	−33:30:37
o1-11	01:00:46.6	−33:30:47
o1-14	01:00:48.0	−33:30:38
o1-6	01:00:43.8	−33:29:08
o1-15	01:00:49.1	−33:29:45
o1-21	01:00:50.4	−33:29:08
o1-22	01:00:50.8	−33:27:52
o1-30	01:00:57.9	−33:27:53
o2-28	00:59:29.0	−33:49:12
o2-25	00:59:27.9	−33:48:59
o2-33	00:59:31.8	−33:47:45
o2-38	00:59:32.6	−33:46:18
o2-46	00:59:33.8	−33:45:05
o2-44	00:59:33.6	−33:44:32

Table A2. Fornax positions.

Star	RA	Dec. (J2000)
c1-660	02:39:51.3	−34:29:58
c1-350	02:39:50.8	−34:29:28
c1-444	02:39:52.3	−34:29:06
c1-371	02:39:51.2	−34:28:44
c1-601	02:39:54.4	−34:28:27
c1-628	02:39:54.8	−34:28:01
c1-564	02:39:53.9	−34:27:37
c1-433	02:39:52.2	−34:27:19
c1-365	02:39:51.1	−34:26:49
c1-122	02:39:47.5	−34:26:30
c1-125	02:39:47.6	−34:26:10
c1-214	02:39:49.0	−34:25:50
c1-360	02:39:51.1	−34:25:17
c1-200	02:39:48.8	−34:24:56
c1-344	02:39:50.9	−34:24:30
c2-822	02:40:10.8	−34:29:45
c2-777	02:40:10.0	−34:29:24
c2-838	02:40:11.0	−34:29:03
c2-828	02:40:10.9	−34:28:56
c2-702	02:40:09.0	−34:28:41
c2-613	02:40:07.9	−34:28:25
c2-769	02:40:10.0	−34:27:56
c2-511	02:40:06.7	−34:27:39
c2-623	02:40:08.1	−34:27:13
c2-388	02:40:05.1	−34:26:53
c2-384	02:40:05.0	−34:26:51
c2-294	02:40:03.7	−34:26:33
c2-552	02:40:07.2	−34:26:05
c2-249	02:40:03.1	−34:25:46
c2-413	02:40:05.4	−34:25:20
c2-647	02:40:08.5	−34:24:53
c2-621	02:40:08.2	−34:24:30
c2-41	02:40:00.2	−34:24:29

Table A3. NGC 6822 Positions.

Star	RA	Dec. (J2000)
s1-309	19:44:47.5	−14:47:00
s1-186	19:44:47.7	−14:46:41
s1-212	19:44:48.2	−14:45:09
s1-210	19:44:48.2	−14:45:06
s1-200	19:44:47.9	−14:44:43
s1-59	19:44:44.8	−14:44:18
s1-188	19:44:47.7	−14:43:39
s1-153	19:44:47.1	−14:43:17
s1-43	19:44:44.5	−14:42:58
s1-205	19:44:48.1	−14:42:14
s1-204	19:44:48.1	−14:42:02
s1-378	19:44:52.0	−14:41:43
s1-111	19:44:46.7	−14:41:21
s1b-280	19:44:49.7	−14:44:49
s2-208	19:45:02.3	−14:45:55
s2-246	19:45:03.4	−14:45:31
s2-263	19:45:09.8	−14:45:10
s2-352	19:45:05.7	−14:44:51
s2-354	19:45:05.7	−14:44:45
s2-250	19:45:03.5	−14:44:02
s2-271	19:45:04.0	−14:43:45
s2-142	19:45:00.8	−14:43:12
s2-248	19:45:03.5	−14:43:00
s2-117	19:45:00.2	−14:42:07
s2-199	19:45:02.1	−14:41:51
s2-198	19:45:02.1	−14:41:39

This paper has been typeset from a TEX/LATEX file prepared by the author.